



OPEN ACCESS

EDITED BY

Fabrice Brunet,
UMR5275 Institut des Sciences de la Terre
(ISTERRE), France

REVIEWED BY

Alessandro Cavallo,
University of Milano-Bicocca, Italy
Martin Li,
Imperial College London, United Kingdom

*CORRESPONDENCE

Abdulrahman M. Alotaibi,
✉ aotaibi@kacst.gov.sa

RECEIVED 02 January 2025

ACCEPTED 03 April 2025

PUBLISHED 02 May 2025

CITATION

Aljabbab A, Qadrouh AN, Alajmi MS,
Alotaibi AM, Baioumy H, Alyousif MM, Bin
Rogaib AM, Fal M and Alkhammali SA (2025)
Composition, origin, and potential industrial
applications of REEs-rich authigenic kaolinite
separated from the Lower Cretaceous white
sands, Saudi Arabia.

Front. Earth Sci. 13:1554712.

doi: 10.3389/feart.2025.1554712

COPYRIGHT

© 2025 Aljabbab, Qadrouh, Alajmi, Alotaibi,
Baioumy, Alyousif, Bin Rogaib, Fal and
Alkhammali. This is an open-access article
distributed under the terms of the [Creative
Commons Attribution License \(CC BY\)](https://creativecommons.org/licenses/by/4.0/). The
use, distribution or reproduction in other
forums is permitted, provided the original
author(s) and the copyright owner(s) are
credited and that the original publication in
this journal is cited, in accordance with
accepted academic practice. No use,
distribution or reproduction is permitted
which does not comply with these terms.

Composition, origin, and potential industrial applications of REEs-rich authigenic kaolinite separated from the Lower Cretaceous white sands, Saudi Arabia

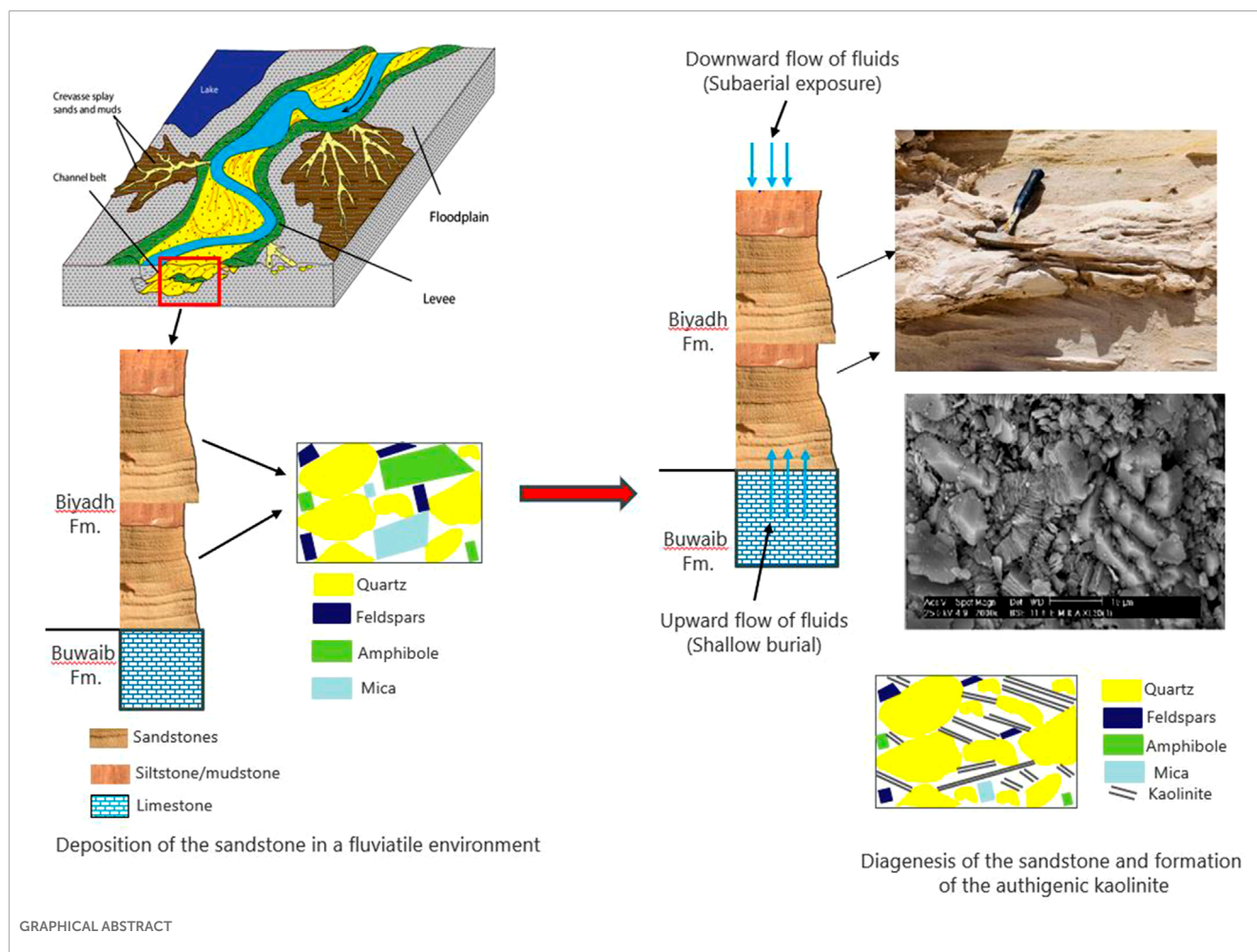
Abdulrahman Aljabbab¹, Ayman N. Qadrouh¹,
Mamdoh S. Alajmi², Abdulrahman M. Alotaibi^{1*},
Hassan Baioumy³, Mazen M. Alyousif¹, Abdulrahman M. Bin
Rogaib¹, Mokhtar Fal⁴ and Sultan A. Alkhammali¹

¹King Abdulaziz City for Science and Technology (KACST), Mining and Hydrocarbon Technologies Institute, Riyadh, Saudi Arabia, ²King Abdulaziz City for Science and Technology (KACST), Carbon Management Institute, Riyadh, Saudi Arabia, ³Natural Resources, Arabian Geophysical and Surveying Co. (ARGAS), Dhahran, Saudi Arabia, ⁴King Abdulaziz City for Science and Technology (KACST), Climate Technologies Institute, Riyadh, Saudi Arabia

The white sands from the Cretaceous Biyadh Formation, Saudi Arabia, are exploited as a raw material for the glass sand industry and contain approximately 15 wt% kaolinite. SEM reveals that the kaolinite develops as a blocky, pore-filling cement of euhedral, pseudo-hexagonal plates ranging from 5 to 10 μm in width and from 10 to 20 μm in length, suggesting its authigenic origin during the late diagenesis. Anatase occurs as very fine grains interspersed among the kaolinite flakes. The authigenic kaolinite is associated with remarkably high concentrations of rare earth elements (REEs) (average 1,126 ppm), Zr (average 1,133 ppm), and Li (average 187 ppm). REEs occur as the phosphate phase, while Zr is associated with the anatase, and Li is hosted by kaolinite. These high concentrations are probably due to the enrichment of these elements during the diagenesis of the studied kaolinite. Alteration of the source minerals during periods of subaerial exposure and/or at shallow burial depths due to meteoric water influx is deduced as a possible mechanism for the formation of the studied kaolinite. The supergene origin of the kaolinite is confirmed by the relatively high concentrations of Ti and Ce + Y + La. The geochemistry and large crystal size suggest the potential application of the kaolinite in paper coating and as a filler. While the high Al_2O_3 and low SiO_2 contents suggest its potential application in super-standard porcelain and sanitary ware, partial removal of TiO_2 will allow its application in the pharmaceutical and cosmetics industries. Additionally, REEs, Zr, and Li can be separated from the white sands as valuable byproducts, along with the kaolinite.

KEYWORDS

kaolinite, white sands, Saudi Arabia, origin, rare earth elements, industrial applications



1 Introduction

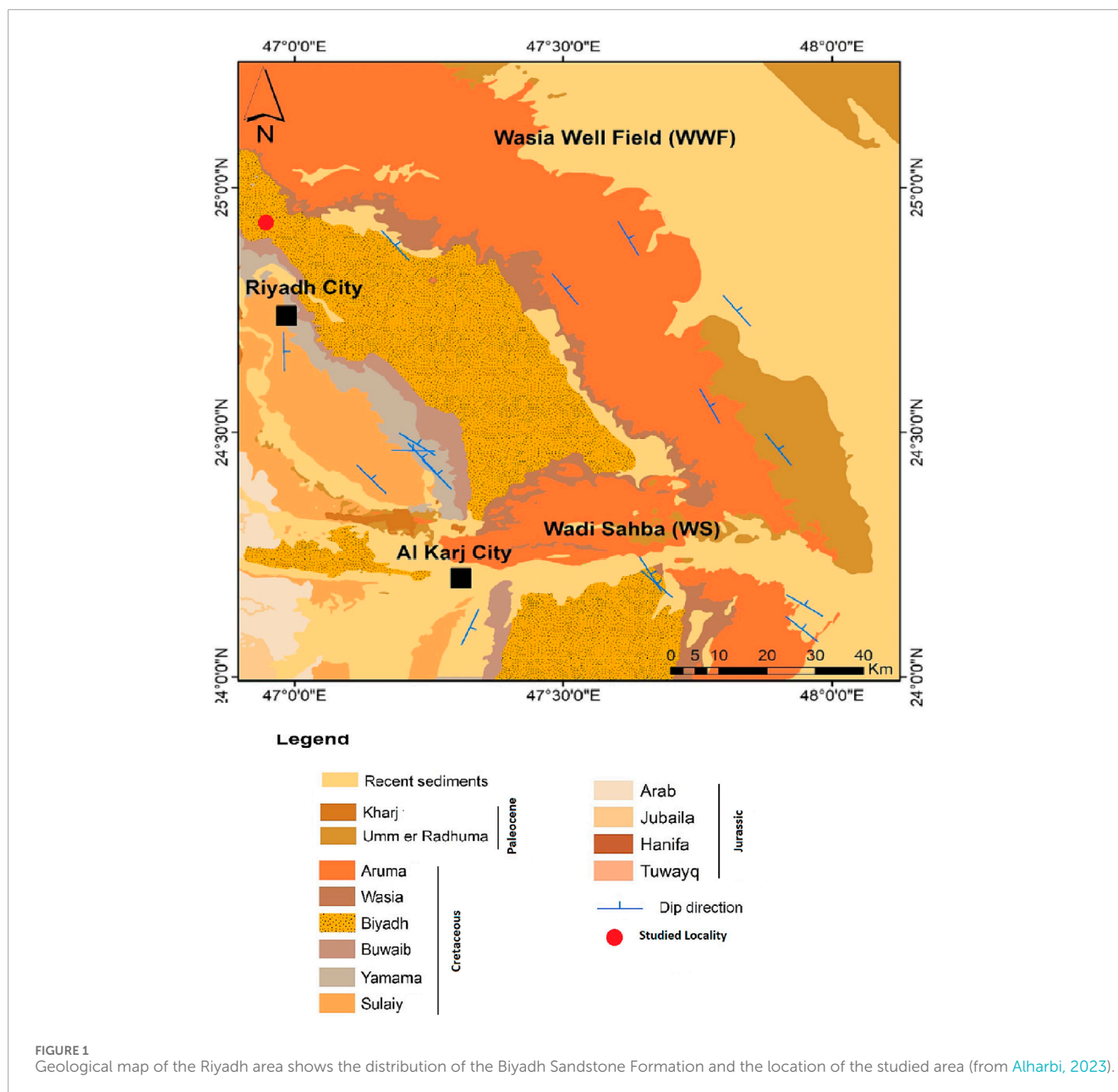
Authigenic minerals (e.g., clay, carbonate, and quartz) are generally formed during progressive diagenesis in siliciclastic rocks (Anjos et al., 2000; Ma et al., 2017; Taylor et al., 2010). Authigenic kaolinite that occurs as grain-rimming and/or pore-filling is pervasively developed in aluminosilicate-rich sandstone (Dill et al., 2022; Dill et al., 2009; Ma et al., 2020; Meng et al., 2020; Waldmann and Gaupp, 2016). The source and formation mechanism of this authigenic kaolinite have been debated for decades (Bjørlykke and Jahren, 2012; Chuhan et al., 2001; Ma et al., 2016; Ma et al., 2021). It has been proposed that authigenic kaolinite precipitated in a geochemically open system due to high invasion of acidic waters flowing extensively into the siliciclastic rocks, with dissolved ions being transported out of the system over long distances (Lanson et al., 2002; Meng et al., 2020; Van Keer et al., 1998). Alternatively, it has been proposed that authigenic kaolinite can form under the very low velocity of pore-fluids in a geochemically closed system, and the dissolved ions precipitate *in situ* or move for very short distances in the system (Bjørlykke and Jahren, 2012; Chuhan et al., 2001; Ma et al., 2016).

White sands have an economic value as a raw material for several industries such as glass, foundry, ceramics, and water filtration (Platiasa et al., 2014). The physical and chemical properties of

these sands are critical in deciding their quality and industrial uses and, therefore, their economic value. Alumina is one of the main impurities in these sands coming from the authigenic kaolinite and reduces their quality. The separation of kaolinite from these sand deposits will improve the physico-chemical characteristics of these sands along with the economic value of the separated kaolinite that can be used as a raw material for several other industries such as ceramic, paper, abrasive, paint, and plastic (Nouri and Masoumi, 2020).

In addition to its common applications (e.g., filler in polymers, rubber, paper, cosmetics, and medicines; Murray, 2006; Murray and Kogel, 2005), kaolinite is used in new technologies such as green nanotechnology to improve human life and solve environmental and economic problems, for storage and production of clean energy via simple and economical methods, and for sustainability. It can be used in composites, nano-hybrids, adsorbents (Dedzo and Detellier, 2014; Matusik and Bajda, 2013; Matusik and Matykovska, 2014), electrode coatings (Tonlé et al., 2011), and catalysts (Araújo et al., 2014; Bizaia et al., 2009; De Faria et al., 2012; Nakagaki et al., 2006).

White sand deposits are extensively distributed in the Middle East and are of different ages such as the Paleozoic and Lower Cretaceous white sands in Egypt (Bandel et al., 1987; Beall and Squyres, 1980; Ibrahim et al., 2018; EL-Wekeil and Gaafar, 2014; Wanas, 2011), Lower Cretaceous glass sands in Jordan (Powell, 1989;



Powers et al., 1966), and Lower Cretaceous white sands in Saudi Arabia (Alharbi, 2023; Le Nindre et al., 2023; Boukhamsin et al., 2023; Keller et al., 2019). The characterization of the authigenic kaolinite has been carried out for the Egyptian (Al-Abady, 2022; EL Sayed et al., 2018) and Jordanian (Alali, 2020) white sands. However, the authigenic kaolinite fraction from the Saudi white sand deposits has not been investigated so far, and previous studies have focused on the white sand deposits (Al-Harbi et al., 1995; Howari, 2015; Mahmoud et al., 2022) without addressing the authigenic kaolinite in these sands. Additionally, the previous studies on the authigenic kaolinite have focused on its origin, morphology, and effect on the porosity and permeability of the host sandstone reservoirs (Fan, et al., 2019; Gao et al., 2022; Lanson, et al., 2002). However, the geochemical characteristics of this kaolinite were not investigated. This study aims, therefore, to determine the

mineralogical and geochemical characteristics of the authigenic kaolinite separated from the Lower Cretaceous white sand deposits of the Biyadh Formation, Saudi Arabia, and examine its source, origin, and suitability for various industrial applications.

2 Geological setting

The Biyadh sandstone was initially specified in the Ar Riyadh quadrangle by Steineke et al. (1958) (Figure 1). In a complete stratigraphic sequence, the Biyadh sandstone is underlain by the Buwaib Formation and overlain by the Sallah Formation (Figure 2A).

According to Le Nindre et al. (2008), the redefined Biyadh sandstone formation exhibits a homogeneous lithology in the

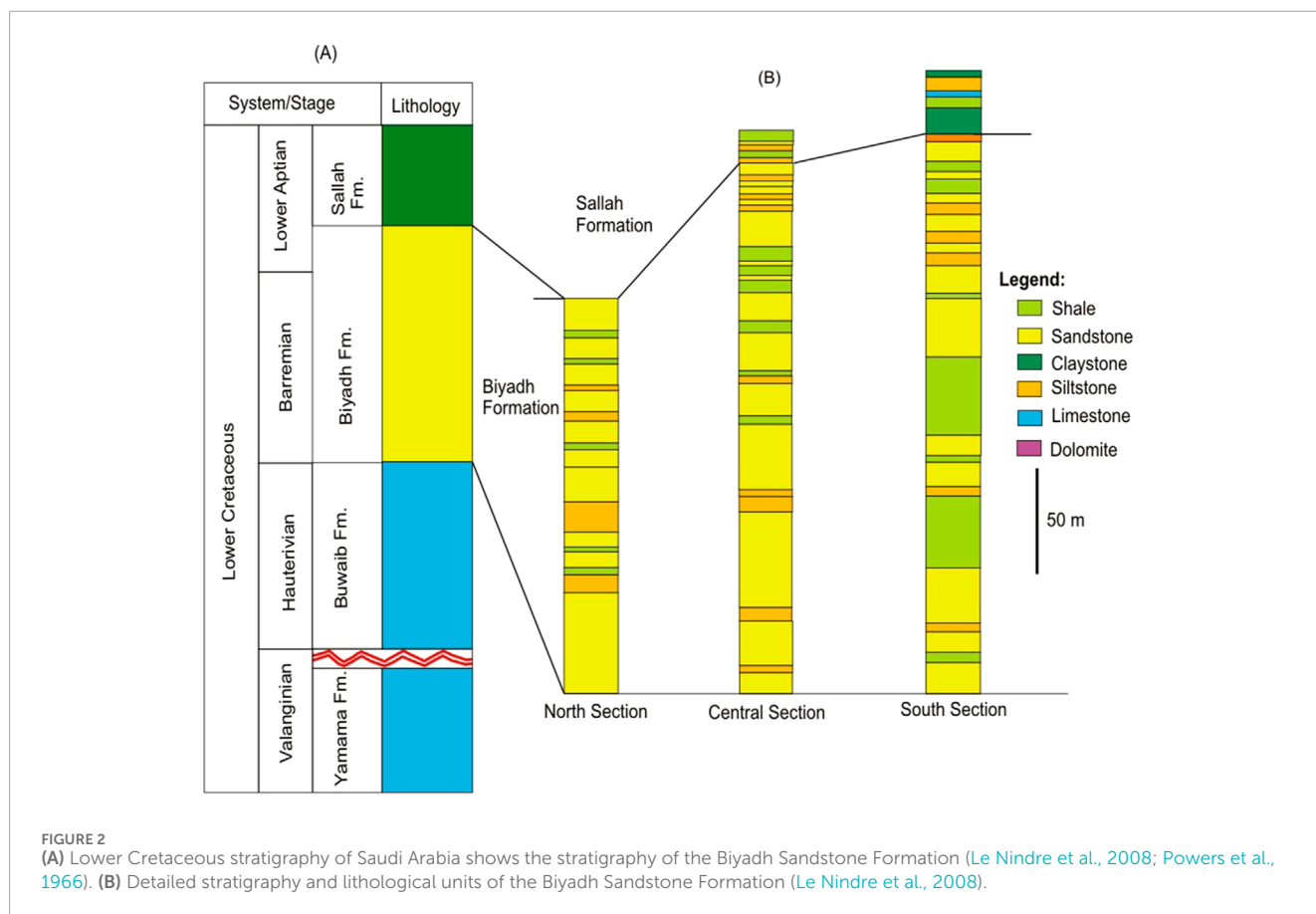


FIGURE 2 (A) Lower Cretaceous stratigraphy of Saudi Arabia shows the stratigraphy of the Biyadh Sandstone Formation (Le Nindre et al., 2008; Powers et al., 1966). (B) Detailed stratigraphy and lithological units of the Biyadh Sandstone Formation (Le Nindre et al., 2008).

Ar Riyadh quadrangle, as indicated in the north, central, and south sections (Figure 2B). In its south section, the Biyadh sandstone formation consists of the following lithostratigraphic units, from base to top: (1) (60 m thick): Light brown to brown, black-weathered, coarse-to-fine-grained, ferruginized, cross-stratified sandstone, with conglomeratic sandstone at the base of troughs (channel lags), including silicified wood and quartz gravel. The assemblage is intercalated with thin beds of white gypsiferous claystone and red to gray siltstone. (2) (110 m thick): Gray, red, or violet siltstone, light brown fine-grained cross-stratified sandstone, and white clayey siltstone, displayed in a meter-scale fining-upward sequences. Coarse-grained sandstone to conglomerate occurs at the base of the succession. (3) (56 m thick): A cross-bedded, fining upward sequence of coarse-grained conglomeratic sandstone, white or brown coarse-to-fine-grained sandstone, white silty claystone, and gray to red siltstone. An intensely reworked gravelly channel lag containing 4-m-long silicified tree trunks is present at the bottom of this unit. (4) (54 m thick): White, gray, or red silty claystone and siltstone with channels filled by coarse-to-fine-grained ferruginized sandstone.

The Biyadh Formation was dated in the subsurface as Barremian, early Aptian, based on the presence of foraminifers *Choffatella decipiens*, *Orbitolina discoidea*, and *Dictyoconous arabicas* (Powers et al., 1966). The depositional environment of the Biyadh Formation is interpreted as the fluvial and lacustrine environment (Moshrif, 1980).

3 Materials and methods

Fifteen samples were collected from several outcrops of the Biyadh sandstone formation (Figures 1, 2). Clay fractions ($<2 \mu\text{m}$) from the sandstones were separated and prepared following the technique described in Baioumy et al. (2012). A 10-g sample of the bulk clays was soaked in distilled water for ~ 2 weeks. During this stage, the samples were ultrasonically treated three times (10–15 min each time) using a cleaning ultrasonic tool and then washed many times with distilled water until a complete suspension was achieved, with pH ranging from 7 to 8. To prevent the contamination of clay fractions, no dispersant chemicals were used. The clay fractions ($<2 \mu\text{m}$) were separated from the aqueous suspensions after ~ 7 h to ensure their purity and dried at 100°C in a drier. The clay powders were then analyzed for their mineralogy and geochemistry. The mineralogical analysis was conducted using a Cu-K α Empyrean X-ray Diffractometer operated at 25 mA and 40 kV at the Central Metallurgical R&D Institute (CMRDI), Egypt. The identification of mineral phases was based on Moore and Reynolds (1989). The quantitative mineralogical compositions were determined using the Rietveld program BGMN1 (Kleeberg and Bergmann, 1998). The degree of structural disorder of the kaolinite was assessed using the Hinckley index (HI) (Hinckley, 1963; Galan et al., 1994). The scanning electron microscope observations have been conducted using SEM-EDX Jeol-JSM 5410 at the National Research Center, Egypt.

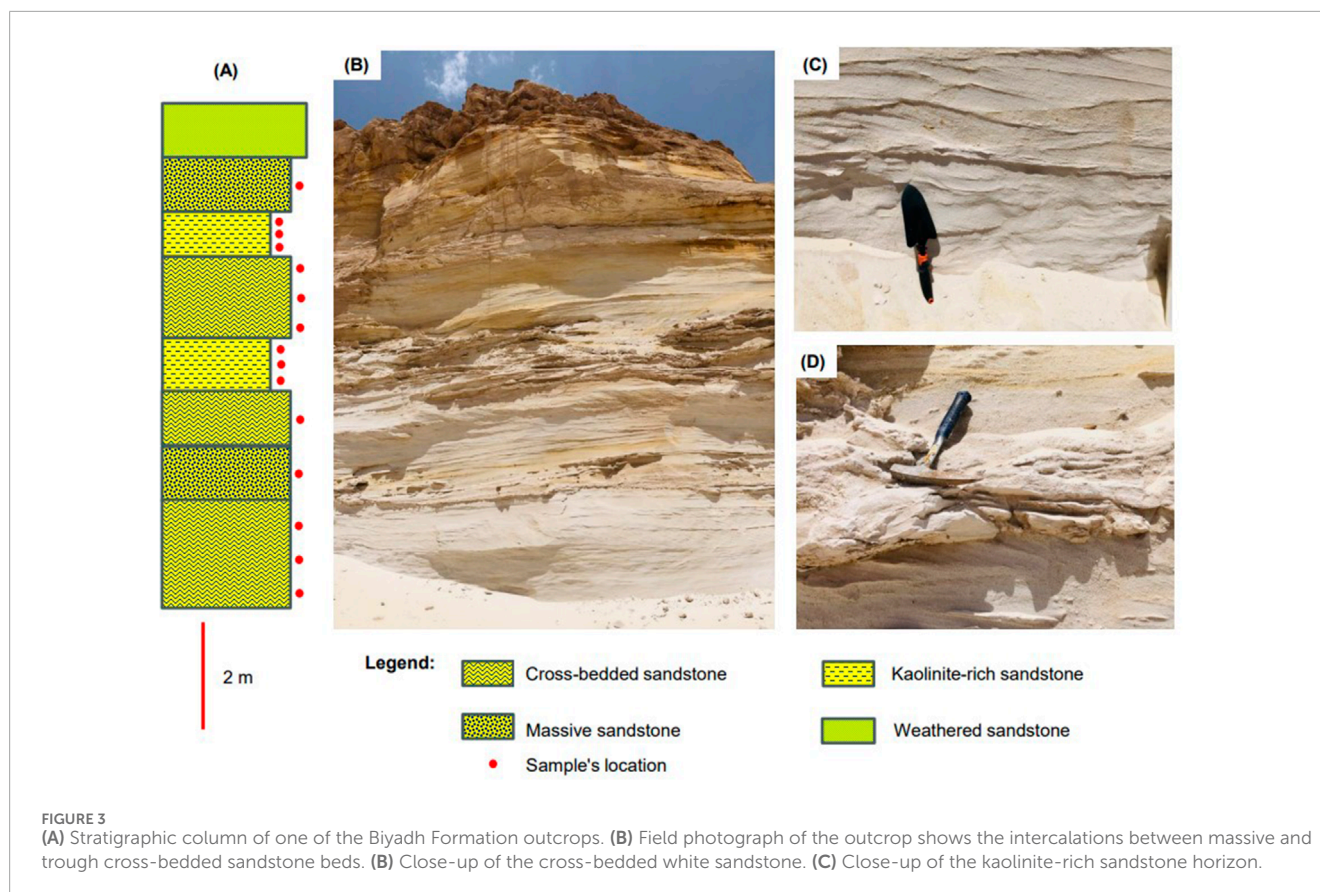


FIGURE 3

(A) Stratigraphic column of one of the Biyadh Formation outcrops. (B) Field photograph of the outcrop shows the intercalations between massive and trough cross-bedded sandstone beds. (C) Close-up of the cross-bedded white sandstone. (D) Close-up of the kaolinite-rich sandstone horizon.

The geochemical analyses, including major oxides and trace and rare earth elements (REEs), of the separated kaolinite samples were conducted at the ALS Lab, KSA. To analyze the major oxides, fused disks were prepared from the sample powders and then analyzed using a Philips PW 2400 X-ray Fluorescence Spectrometer operated at 40 kV and 60 mA. Loss on ignition was calculated after burning the samples at 1,000°C for 3 h. Concentrations of trace elements and REEs were analyzed via inductively coupled plasma optical mass spectrometry (ICP-MS) after complete acid dissolution of the sample powders. The sample powders were first completely dissolved in 38 wt% HF with 68 wt% HNO₃ in capped Teflon vials and heated for 24 h (~150°C) on a hot plate. The resulting solutions were dried using a hot plate at ~150°C and subsequently treated again with 2 mL of HNO₃ (6 mol/L) at 150°C and evaporated to dryness. The residues were then treated with 1 mL of HNO₃, and the solutions were then diluted for analysis (Jenner et al., 1990).

4 Results

4.1 Occurrence and mineralogy of the authigenic kaolinite

The kaolinite-bearing white sandstone of the Biyadh Formation occurs as intercalations between massive and trough cross-bedded sandstone beds (Figures 3A, B). The thicknesses of the sandstone beds vary between 2 and 3.3 m. The sandstones are composed of very fine to fine- and medium-grained, angular, sub-angular to

sub-rounded grains; they are friable, soft, and partially reworked massive white sandstones encompassing scattered quartz pebbles and granules. Kaolinite in these sands occurs as disseminated fine-grained, white, and soft material within the coarser sands (Figure 3C). Under SEM, kaolinite occurs as blocky, pore-filling cement composed of euhedral, pseudo-hexagonal plates measuring 5–10 μm in width and 10–20 μm in length (Figure 4A). EDX analysis of this kaolinite shows the characteristic Si, O, and Al peaks (Figure 4B) without any other impurities in the kaolinite itself. Anatase is the main impurity associated with the kaolinite, occurring as very fine grains (micro to nano-sized) scattered between the kaolinite flakes (Figure 4C). EDX analysis confirmed the presence of anatase by its characteristic Ti Kα peak (Figure 4D). The XRD patterns of the unoriented mounts (Figure 5A) display the typical kaolinite reflections at 12.40°, 20.38°, 24.96°, and 35° (Daou et al., 2020), along with traces of anatase. The HI was calculated from the XRD pattern of the separated authigenic kaolinite (Figure 5B), with values ranging from 1.0 to 1.1 and an average of 1.07, indicating the high crystallinity of this kaolinite. This is also confirmed by the morphology of the kaolinite observed via SEM.

4.2 Geochemistry of the kaolinite separate

4.2.1 Major oxides

The bulk white sands from the Biyadh Formation are characterized by high SiO₂ contents, ranging from 84.3 wt% to 97.5 wt%. The Al₂O₃ contents that reflect mainly the authigenic

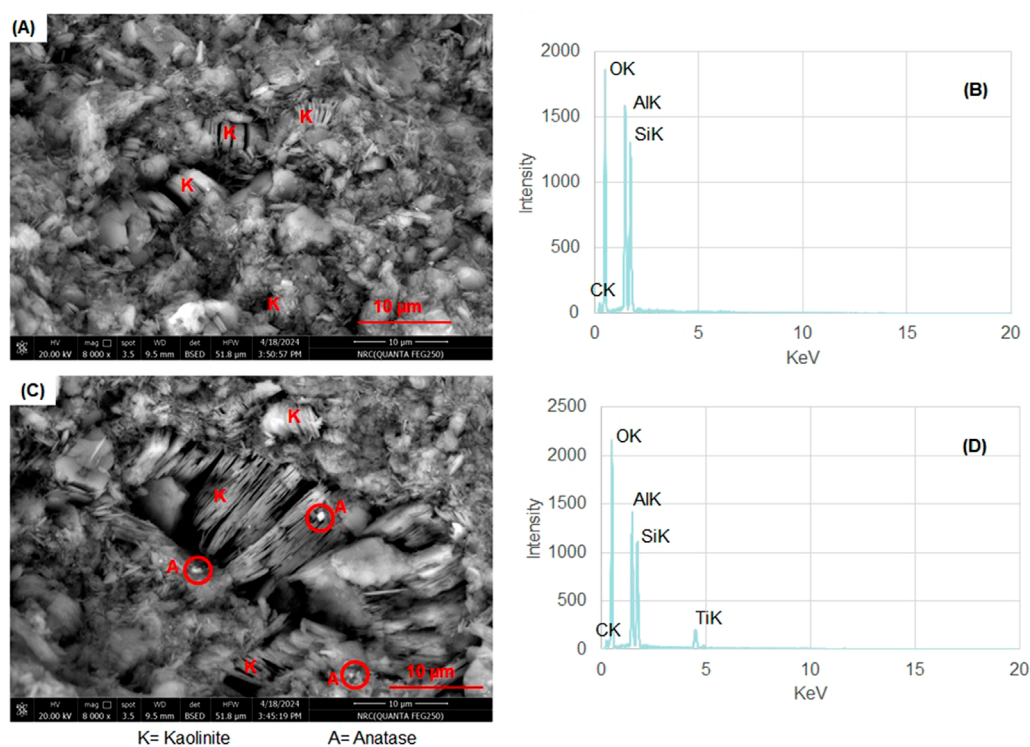


FIGURE 4

(A) SEM photomicrographs of the authigenic kaolinite as blocky, pore-filling cement comprising euhedral, pseudo-hexagonal plates measuring 5–10 µm in width and 10–20 µm in length. (B) EDX analysis for this kaolinite characterized by Si, O, and Al peaks. (C) Anatase occurs as very fine grains (micro to nano-sized) scattered between the kaolinite flakes (red circles). (D) EDX analysis of anatase by its characteristic Ti-K α peak.

kaolinite contents in these sands vary from 1.1 wt% to 6.2 wt% (Al-Harbi et al., 1995). The major oxide contents of the separated authigenic kaolinite from the Biyadh Formation are shown in Table 1. SiO₂ and Al₂O₃ contents represent the major oxide constituents, with SiO₂ ranging from 44.73 wt% to 45.61 wt%, and Al₂O₃ content, which primarily reflects the authigenic kaolinite content in these sands, ranging from 37.97 wt% to 38.70 wt%. The SiO₂ and Al₂O₃ concentrations are typical for pure kaolinite, as shown by the strong positive correlation (Figure 6A) between the two components ($r^2 = 1$), and the SiO₂/Al₂O₃ ratios (1.18). This also confirms that the analyzed samples are close to pure kaolinite, and its separation from the sandstone was carried out precisely without any quartz or any other coarse components from the hot sandstone. TiO₂ represents the major impurity in the separated kaolinite and occurs in relatively high contents (average 1.6 wt%). TiO₂ occurs as very fine anatase, as indicated by the SEM and EDX analyses. The Fe₂O₃ contents range between 0.43 wt% and 0.69 wt%, with an average of 0.54 wt%. Other impurities such as K₂O, MgO, Na₂O, CaO, MnO, and P₂O₅ occur in very low concentrations, each less than 0.1 wt%. All these impurities, including Fe₂O₃ and TiO₂, show a lack of correlations or negative correlations with Al₂O₃ (Figures 6B–E), indicating that these elements are not related to the kaolinite and occur in different phases. SEM and EDX analyses confirmed that, where peaks of these elements have been detected in the EDX analysis of the kaolinite crystals (Figure 4A), Fe₂O₃ correlates positively with TiO₂ (Figure 6E), indicating the presence of iron in the anatase structure replacing Ti.

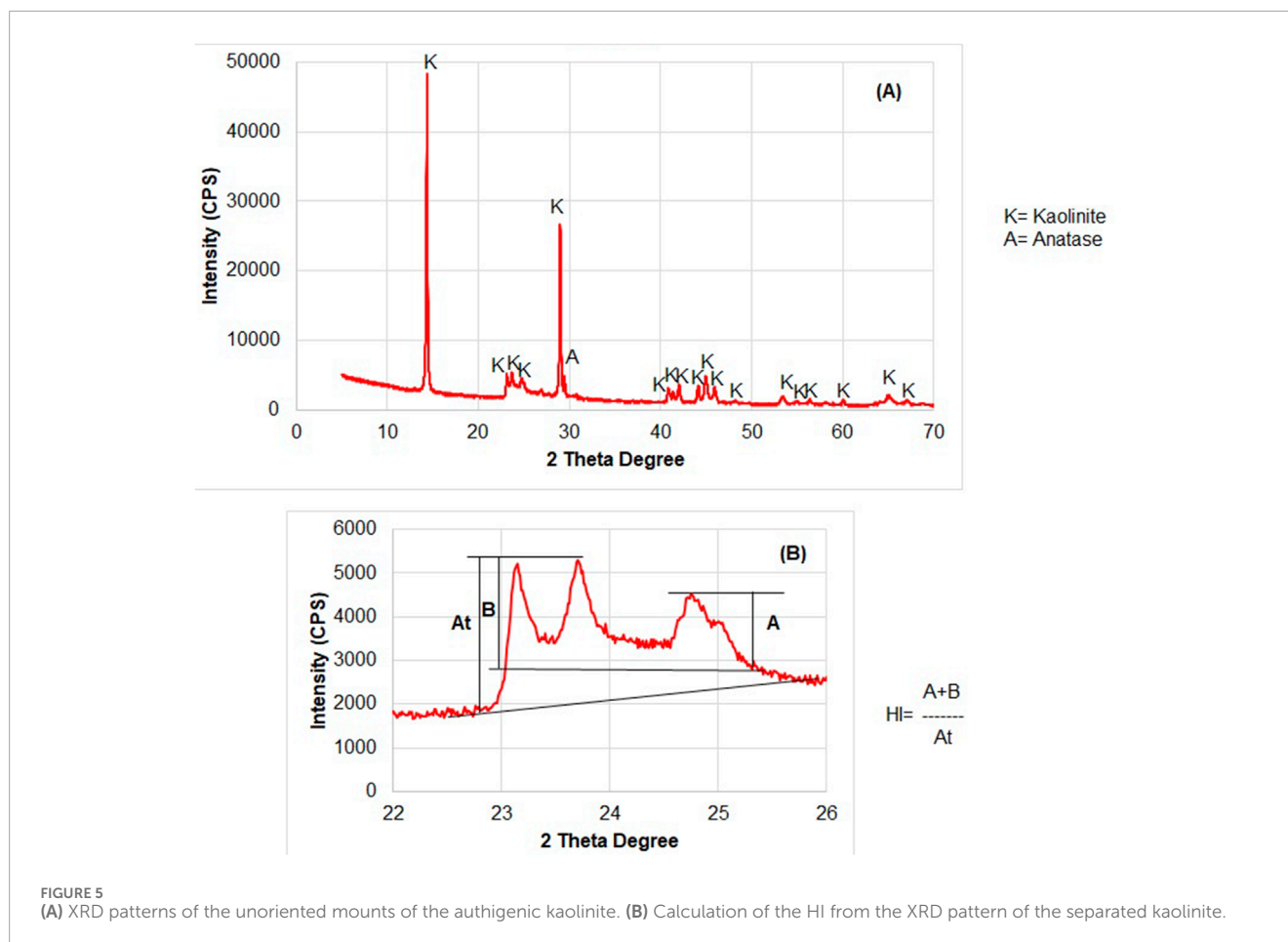
4.2.2 Trace elements

Concentrations of trace elements in the authigenic kaolinite separated from the white sands are listed in Table 2. Zr has the highest concentration, ranging from 841 to 1,510 ppm (average of 1,133 ppm), followed by Sr, which varies between 175 and 378 ppm (average 272 ppm). Cr ranges from 148 to 306 ppm (average 280 ppm), Ba ranges from 73 to 159 ppm (average 111 ppm), Li ranges from 130 to 200 ppm (average 187 ppm), and Pb ranges from 61 to 151 ppm (average 108 ppm). Elements such as Ga, Hf, Nb, Th, V, Y, Ni, Sc, and Zn are present in relatively low concentrations, less than 100 ppm (averages 32, 29, 32, 43, 63, 60, 63, 24, and 20 ppm for Ga, Hf, Nb, Th, V, Y, Ni, Sc, and Zn, respectively). Other elements occur in concentrations lower than 10 ppm, including Ge (1.6 ppm), Rb (0.5 ppm), Sn (3 ppm), Ta (2 ppm), U (4 ppm), W (2 ppm), As (0.2 ppm), Co (2.5 ppm), and Cu (6 ppm).

Only Li correlates positively with Al₂O₃ (Figure 7A), indicating its direct association with the kaolinite. However, many of the trace elements, such as Zr, Nb, V, Y, Ta, and U, exhibit positive correlations with TiO₂ (Figures 7B–D). Nb, V, Sn, and Ta exhibit positive correlations with Fe₂O₃ (Figures 7E, F), while Ba, Sr, Pb, Th, Ni, and Sc exhibit positive correlations with P₂O₅ (Figures 7G, H).

4.2.3 Rare earth elements

Concentrations of REEs in the authigenic kaolinite separated from the white sands are shown in Table 3. The Σ REEs varies between 715 and 1,675 ppm (average 1,126 ppm). Σ REEs do not



correlate with Al_2O_3 (Figure 8A), suggesting that the majority of REEs are not associated with the kaolinite. Meanwhile, REEs correlate positively with P_2O_5 (Figure 8B), indicating that REEs occur in a minor phosphate phase. The phosphate phase was not observed using XRD (i.e., below detection). Chondrite-normalized REE patterns of the authigenic kaolinite using chondrite values (Boynton, 1984) are shown in Figure 8C. Ce and Eu anomalies were also calculated following the method described by Boynton (1984). REE chondrite-normalized patterns in the authigenic kaolinite samples display similar general patterns with higher light rare earth elements (LREEs) compared to heavy rare earth elements (HREEs), as indicated by $(\text{La}/\text{Yb})_n$ ratios that vary between 19 and 31. The kaolinite samples show that negative Eu anomalies (Eu/Eu^*) vary from 0.74 to 0.79 and slight negative Ce anomalies (Ce/Ce^*) range between 0.95 and 0.97.

5 Discussion

5.1 Source and formation mechanism of the kaolinite

As suggested by the previous studies (Arditto, 1983; Berger et al., 1997; Chen et al., 2019; Gao et al., 2022; Ma et al., 2017; Mansurbeg et al., 2008; Meng et al., 2020; Morad et al., 2010), the

dissolution of feldspars is the main source of authigenic kaolinite cementation in the Biyadh sandstones.

Kaolinite in the Biyadh Formation occurs mainly as pore-filling cement located between the quartz grains (Figure 4), suggesting the authigenic origin of this kaolinite formed during later stages of diagenesis (Marfil et al., 2003). The alteration of aluminosilicates to kaolinite in the sandstones occurs under a wide range of conditions: (i) during the subaerial exposure of the sandstones; (ii) at shallow burial depth (generally < 1 km) due to the influx of meteoric water; and (iii) deeper (2–4 km) through the interaction with acidic water from the thermal maturation of organic matter (Curtis, 1983; Surdam et al., 1984). The Biyadh Formation is bounded by limestone and intercalated with shales, and no organic-rich sediments are associated with this formation. Hence, the formation of kaolinite in the Biyadh sandstones through the interaction of source minerals with acidic water from the thermal maturation of organic matter is not applicable. Hence, alteration of the source minerals during the subaerial exposure of the Biyadh sandstones and/or at shallow burial depth due to the influx of meteoric water is the possible formation mechanism of the authigenic kaolinite in the Biyadh Formation.

Binary plots of $\text{Ba} + \text{Sr}$ vs. $\text{La} + \text{Ce} + \text{Y}$ and $\text{Cr} + \text{Nb}$ vs. $\text{TiO}_2 + \text{Fe}_2\text{O}_3$ are utilized to distinguish between the supergene and hypogene origin of kaolinization (Dill et al., 1997). These plots show that the studied kaolinite has a supergene origin (Figures 9A, B,

TABLE 1 Major oxide contents (wt%) of the authigenic kaolinite from the Lower Cretaceous Biyadh Formation in Saudi Arabia.

Sample	SiO ₂	Al ₂ O ₃	TiO ₂	Fe ₂ O ₃	CaO	K ₂ O	MgO	MnO	Na ₂ O	P ₂ O ₅	LOI	Total
Detection limit	0.01	0.01	0.01	0.01	0.01	0.01	0.01	0.01	0.01	0.01	0.01	—
B-1	45.31	38.45	1.76	0.52	0.10	0.02	0.07	0.01	0.01	0.17	13.20	99.62
B-2	45.59	38.69	1.18	0.52	0.07	0.01	0.07	0.01	0.01	0.19	13.19	99.53
B-3	45.61	38.70	1.30	0.43	0.06	0.01	0.08	0.01	0.01	0.12	13.52	99.85
B-4	45.50	38.61	1.41	0.49	0.08	0.01	0.07	0.01	0.01	0.16	13.30	99.67
B-5	45.60	38.69	1.25	0.48	0.07	0.01	0.05	0.01	0.01	0.16	13.70	100.03
B-6	45.37	38.50	1.60	0.51	0.10	0.01	0.07	0.01	0.01	0.22	13.56	99.96
B-7	45.46	38.58	1.40	0.46	0.15	0.01	0.08	0.01	0.01	0.22	13.51	99.89
B-8	45.49	38.60	1.41	0.49	0.09	0.01	0.07	0.01	0.01	0.18	13.43	99.79
B-9	44.73	37.96	1.83	0.59	0.14	0.01	0.08	0.01	0.08	0.16	13.49	99.08
B-10	45.19	38.34	1.79	0.69	0.09	0.01	0.07	0.01	0.01	0.26	12.92	99.38
B-11	45.39	38.51	1.49	0.52	0.09	0.01	0.07	0.01	0.02	0.18	13.38	99.68
B-12	45.09	38.26	1.80	0.65	0.10	0.01	0.07	0.01	0.01	0.18	13.26	99.45
B-13	45.33	38.46	1.40	0.55	0.17	0.02	0.09	0.01	0.01	0.18	13.38	99.60
B-14	45.36	38.49	1.51	0.53	0.10	0.01	0.07	0.01	0.02	0.18	13.37	99.66
B-15	45.26	38.40	1.57	0.58	0.12	0.01	0.08	0.01	0.01	0.18	13.34	99.57

respectively), confirming the low-temperature formation conditions of the kaolinite either during subaerial exposure or at shallow burial depths of the sandstones. TiO₂ values are also used to determine the origin of the alteration fluid responsible for the formation of kaolinite. When these values are lower than 1, it implies that the nature of the fluids is hypogenic, and when the values are higher than 1, the nature of the fluids is supergenic (Maiza et al., 2003). The results of geochemical analyses pointed out that all the samples have TiO₂ values greater than 1, which implies that this kaolinite is a supergene solution product. TiO₂ + Fe₂O₃ values in the kaolinite are utilized to interpret the fluid source. When these values are less than 1 and more than 1, they correspond to a kaolinite deposit of hypogene and supergene origin, respectively (Dill et al., 1997; Dill et al., 2000; Stoffregen and Alpers, 1987). Kaolinite samples from the Biyadh Formation have TiO₂ + Fe₂O₃ values greater than 1, which clearly implies a supergene process. The total concentration of Ce, Y, and La is used to differentiate between supergene and hypogene origins of kaolinite, and more than 100 ppm of Ce + Y + La implies a supergene process (Dill et al., 1997; Dill et al., 2000). For the authigenic kaolinite from the Biyadh Formation, all samples represent Ce + Y + La values > 100 ppm, which also implies a supergene process for the kaolinite from the Biyadh Formation.

5.2 High Ti, Zr, Σ REEs, and Li

Σ REEs contents in the authigenic kaolinite separated from the Biyadh Formation range from 715 ppm to 1,675 ppm, with an average of 1,126 ppm. These values are exceptionally high compared to other primary kaolinites, such as the primary kaolinite from Malaysia (derived from granites) with an average Σ REEs of 107 ppm (Baioumy et al., 2021) or the primary kaolinite from the Bohemian Massifs with an average Σ REEs of 285 ppm (Höhn et al., 2014). These values are also higher than those in the secondary kaolinite, such as the Cretaceous kaolinite deposits in Egypt, with an average Σ REEs of 275 ppm (Baioumy et al., 2012; Baioumy, 2014).

The authigenic kaolinite separated from the Biyadh Formation also exhibits high Zr contents, varying from 841 ppm to 1,510 ppm, with an average of 1,133 ppm, and it exhibits a positive correlation with TiO₂, indicating its association with anatase or incorporation within the anatase structure. These Zr contents are extremely higher than those in the plagioclase (average 0.03 ppm), biotite (average 3 ppm), K-feldspars (average 0.2 ppm), and muscovite (average 1.7 ppm) (Fan et al., 2023). These values are also higher than those in other authigenic kaolinites, such as the primary kaolinite from Malaysia (derived from granites), with an average of 5 ppm

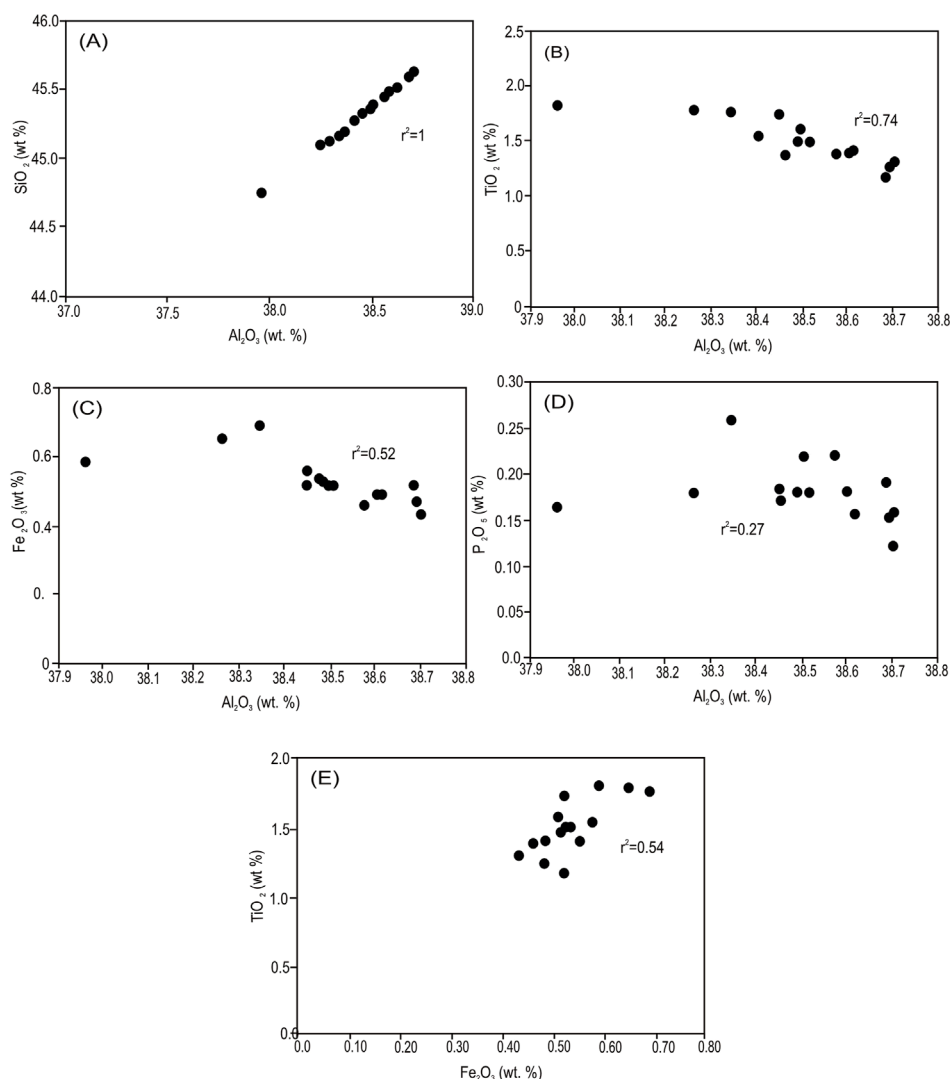


FIGURE 6

(A) Strong positive correlation between SiO₂ and Al₂O₃. (B) Negative correlation between TiO₂ and Al₂O₃. (C) Negative correlation between Fe₂O₃ and Al₂O₃. (D) Lack of correlation between P₂O₅ and Al₂O₃. (E) Fe₂O₃ shows a relatively strong positive correlation with TiO₂.

(Baïoumy et al., 2021), or the primary kaolinite from the Bohemian Massifs, with an average of 254 ppm (Höhn et al., 2014).

Primary kaolinite from Malaysia (Baïoumy et al., 2021) and Bohemian Massifs (Höhn et al., 2014) contains very low Ti contents, with averages of 0.04 and 0.5 wt%, respectively. Additionally, according to Fan et al. (2023), the Ti concentrations in the plagioclase and K-feldspars are also low (averages 40 ppm and 32 ppm, respectively). However, TiO₂ contents in the authigenic kaolinite separated from the Biyadh Formation are high (average 1.6 wt%). SEM and EDX analyses pointed out that Ti in the authigenic kaolinite separated from the Biyadh Formation occurs as anatase. Geochemical correlations implied that several trace elements (e.g., Zr, Nb, V, Y, Ta, and Y) occur in the anatase structure, replacing Ti, as indicated by the positive correlations between these elements and Ti.

The lowest industrial level for sedimentary lithium resources is 260 ppm (Li et al., 2023; Tabelin et al., 2021). The Li content in

authigenic kaolinite from the Biyadh Formation is relatively high, with an average of 187 ppm, which is close to this value. Li is the only trace element that exhibits a positive correlation with Al₂O₃ contents, indicating its association with kaolinite. Nikdel et al. (2024) reported the same trend in the bauxitic kaolin deposits in Iran.

The remarkably high contents of Ti, Zr, REEs, and Li in the authigenic kaolinite separated from the Biyadh Formation are most probably due to their enrichments during the diagenesis of the study kaolinite.

5.3 Possible industrial applications of the kaolinite

5.3.1 Direct applications of the kaolinite

The geochemical and mineralogical characteristics of kaolinite are substantial factors in determining its quality and industrial

TABLE 2 Trace elements contents (ppm) of the authigenic kaolinite from the Lower Cretaceous Biyadh Formation in Saudi Arabia.

Elements	Detection limit	B-1	B-2	B-3	B-4	B-5	B-6	B-7	B-8	B-9	B-10	B-11	B-12	B-13	B-14	B-15
Ba	0.5	103.5	116.0	73.3	97.6	101.5	130.5	130.0	107.5	105.5	158.5	112.4	103.0	110.0	111.5	108.2
Cr	0.01	148.0	306.0	169.0	207.7	198.0	178.0	187.0	199.1	303.0	169.0	206.5	253.0	174.0	207.6	211.5
Ga	0.002	23.5	31.3	29.4	28.1	32.5	30.8	31.9	29.6	35.4	41.0	31.4	33.8	36.2	31.9	34.0
Ge	0.005	2.0	1.7	1.4	1.7	1.5	1.4	1.4	1.6	1.1	1.9	1.6	1.7	1.7	1.6	1.7
Hf	0.002	41.8	23.5	19.9	28.4	19.6	43.8	30.9	29.7	33.5	23.8	29.5	38.0	24.8	29.8	30.9
Nb	0.002	30.6	26.0	23.6	26.7	25.8	33.1	31.1	28.1	51.2	39.8	31.6	41.0	30.7	32.3	34.7
Rb	0.005	0.3	0.4	0.5	0.4	0.5	0.5	0.5	0.4	0.2	0.3	0.4	0.4	1.7	0.5	0.9
Sn		2.4	2.9	2.5	2.6	2.7	2.7	2.4	2.6	3.3	4.5	2.9	3.0	3.7	2.9	3.2
Sr	0.01	256.0	288.0	174.5	239.5	241.0	340.0	319.0	265.4	259.0	378.0	276.0	262.0	253.0	273.2	262.7
Ta	0.005	2.0	1.6	1.5	1.7	1.5	2.2	2.1	1.8	3.1	2.5	2.0	2.7	1.8	2.0	2.2
Th	0.002	38.9	46.9	33.0	39.6	40.9	51.8	46.3	42.5	30.4	59.5	43.0	38.0	47.9	43.0	43.0
U	0.001	4.8	3.7	2.9	3.8	3.1	4.8	3.8	3.8	4.4	4.7	4.0	5.2	3.9	4.1	4.4
V	0.1	64.0	53.0	57.0	58.0	55.0	62.0	60.0	58.4	80.0	73.0	62.0	70.0	60.0	62.5	64.2
W	0.001	1.8	1.2	1.4	1.5	3.1	1.9	1.4	1.8	2.5	1.8	1.8	2.6	1.5	1.9	2.0
Y	0.003	62.9	57.4	52.7	57.7	43.8	69.0	60.8	57.8	70.3	63.4	59.6	66.7	53.6	59.7	60.0
Zr	0.01	1450.0	898.0	854.0	1067.3	841.0	1290.0	1075.0	1067.9	1350.0	1198.0	1109.1	1510.0	957.0	1128.3	1198.4
As	0.01	0.4	0.2	0.1	0.2	0.1	0.1	0.1	0.2	0.2	0.2	0.2	0.2	0.4	0.2	0.3
Co	0.001	2.0	3.0	1.0	2.0	3.0	3.0	3.0	2.4	3.0	2.0	2.4	3.0	2.0	2.5	2.5
Cu		7.0	5.0	5.0	5.7	5.0	6.0	6.0	5.7	5.0	8.0	5.8	5.0	7.0	5.9	6.0
Li	0.1	200.0	200.0	200.0	200.0	200.0	190.0	200.0	198.6	130.0	180.0	189.9	170.0	180.0	187.6	179.2
Ni	0.04	36.0	41.0	27.0	34.7	34.0	46.0	40.0	37.0	30.0	40.0	36.6	38.0	32.0	36.3	35.4
Pb	0.005	105.0	118.0	61.0	94.7	97.0	138.0	133.0	106.7	91.0	151.0	109.5	107.0	99.0	108.5	104.8
Sc	0.005	25.0	24.0	16.0	21.7	20.0	31.0	25.0	23.2	19.0	33.0	23.8	24.0	25.0	23.9	24.3
Zn	0.1	23.0	26.0	15.0	21.3	22.0	18.0	17.0	20.3	16.0	21.0	20.0	16.0	21.0	19.7	18.9

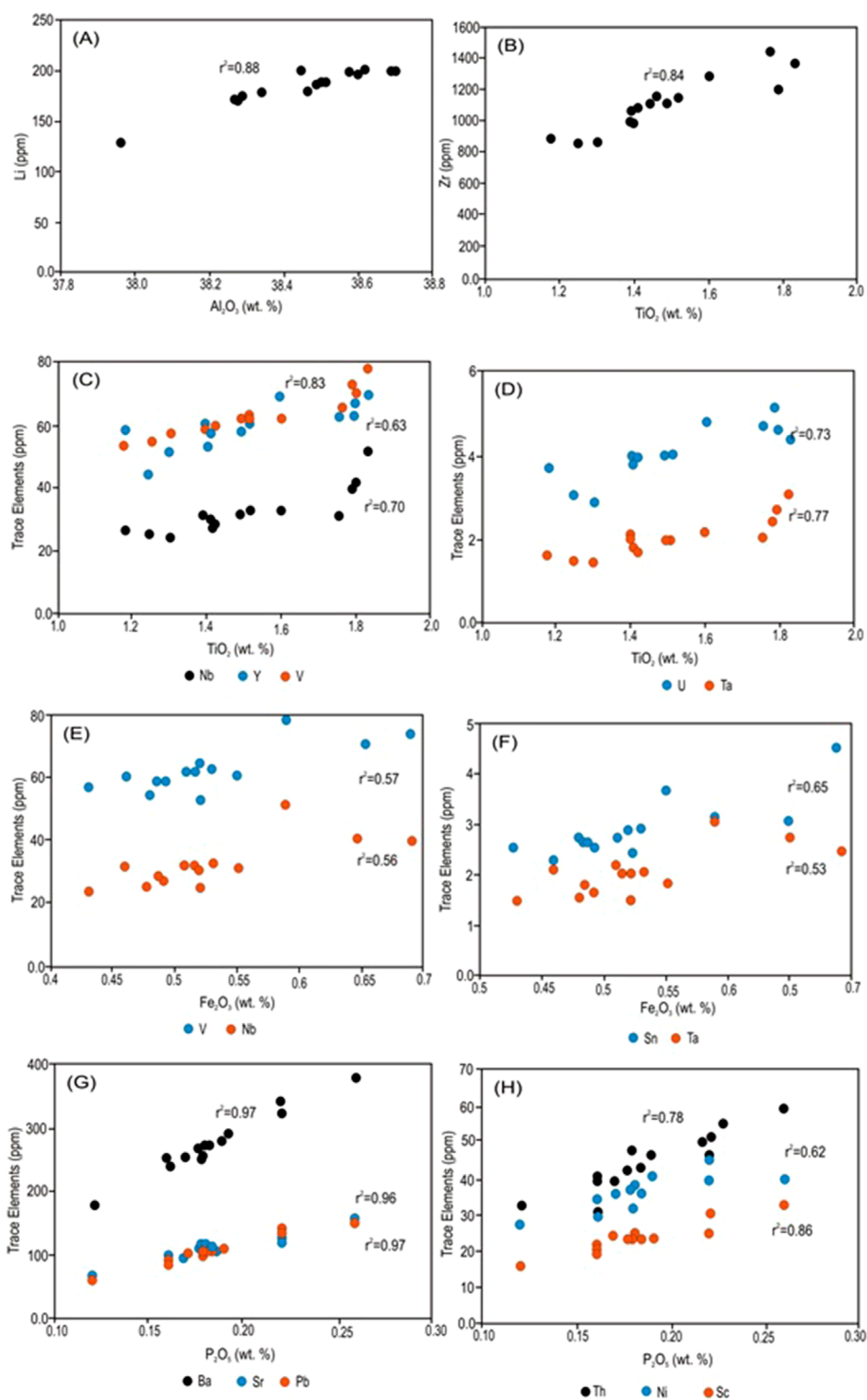


FIGURE 7

(A) Li positively correlates with Al_2O_3 . (B) Positive correlation between TiO_2 and Zr. (C) Positive correlation between TiO_2 and Nb, V, and Y. (D) Positive correlation between TiO_2 and Ta and U. (E) Nb and V exhibit positive correlations with Fe_2O_3 . (F) Sn and Ta exhibit positive correlations with Fe_2O_3 . (G) Ba, Sr, and Pb show positive correlations with P_2O_5 . (H) Th, Ni, and Sc show positive correlations with P_2O_5 .

TABLE 3 Rare earth element contents (ppm) of the authigenic kaolinite from the Lower Cretaceous Biyadh Formation in Saudi Arabia.

Sample	La	Ce	Pr	Nd	Sm	Eu	Gd	Tb	Dy	Ho	Er	Tm	Yb	Lu	Sum	Ce/Ce*	Eu/Eu*
Detection limit	0.001	0.003	0.0005	0.002	0.001	0.0005	0.0005	0.0005	0.0005	0.0005	0.0005	0.0005	0.0001	0.0005	—	—	—
B-1	209.0	426.0	43.9	169.5	30.6	6.3	20.8	2.6	13.1	2.1	6.2	0.9	6.5	1.1	938.5	0.97	0.77
B-2	269.0	542.0	57.9	224.0	43.5	8.5	26.5	3.1	15.2	2.4	6.9	0.9	6.7	1.0	1207.5	0.95	0.76
B-3	155.5	316.0	34.5	135.0	26.1	5.4	18.0	2.1	10.6	1.7	4.7	0.7	4.9	0.7	715.9	0.96	0.77
B-4	211.2	428.0	45.4	176.2	33.4	6.8	21.8	2.6	12.9	2.1	5.9	0.8	6.1	0.9	954.0	0.96	0.77
B-5	228.0	463.0	49.1	189.0	37.5	7.1	23.4	2.6	12.0	2.0	5.3	0.7	5.5	0.8	1026.0	0.96	0.74
B-6	307.0	627.0	65.9	252.0	48.2	9.9	30.1	3.7	17.6	2.9	8.1	1.1	8.5	1.2	1383.2	0.97	0.79
B-7	301.0	610.0	63.8	245.0	44.1	9.0	28.0	3.2	16.0	2.5	7.1	0.9	6.6	1.0	1338.3	0.96	0.77
B-8	240.1	487.4	51.5	198.7	37.6	7.6	24.1	2.8	13.9	2.2	6.3	0.9	6.4	1.0	1080.5	0.96	0.78
B-9	223.0	454.0	48.7	193.5	39.9	8.2	26.4	3.2	16.7	2.7	7.6	1.1	7.8	1.2	1034.1	0.96	0.77
B-10	359.0	748.0	80.7	323.0	66.0	12.8	40.4	4.5	20.6	3.0	7.9	1.0	7.3	1.1	1675.3	0.96	0.78
B-11	250.3	510.1	54.1	210.6	40.7	8.2	25.9	3.0	14.8	2.3	6.6	0.9	6.6	1.0	1135.3	0.97	0.76
B-12	248.0	505.0	53.6	204.0	40.8	8.1	26.9	3.2	16.2	2.7	7.7	1.1	7.5	1.1	1125.8	0.97	0.75
B-13	232.0	468.0	50.0	193.5	37.5	7.6	24.8	2.9	14.4	2.3	6.3	0.9	6.3	1.0	1047.4	0.96	0.76
B-14	248.7	506.5	53.8	208.8	40.5	8.1	25.9	3.0	14.9	2.4	6.7	0.9	6.7	1.0	1127.8	0.96	0.77
B-15	242.9	493.2	52.5	202.1	39.6	7.9	25.9	3.0	15.2	2.5	6.9	1.0	6.8	1.1	1100.4	0.96	0.76

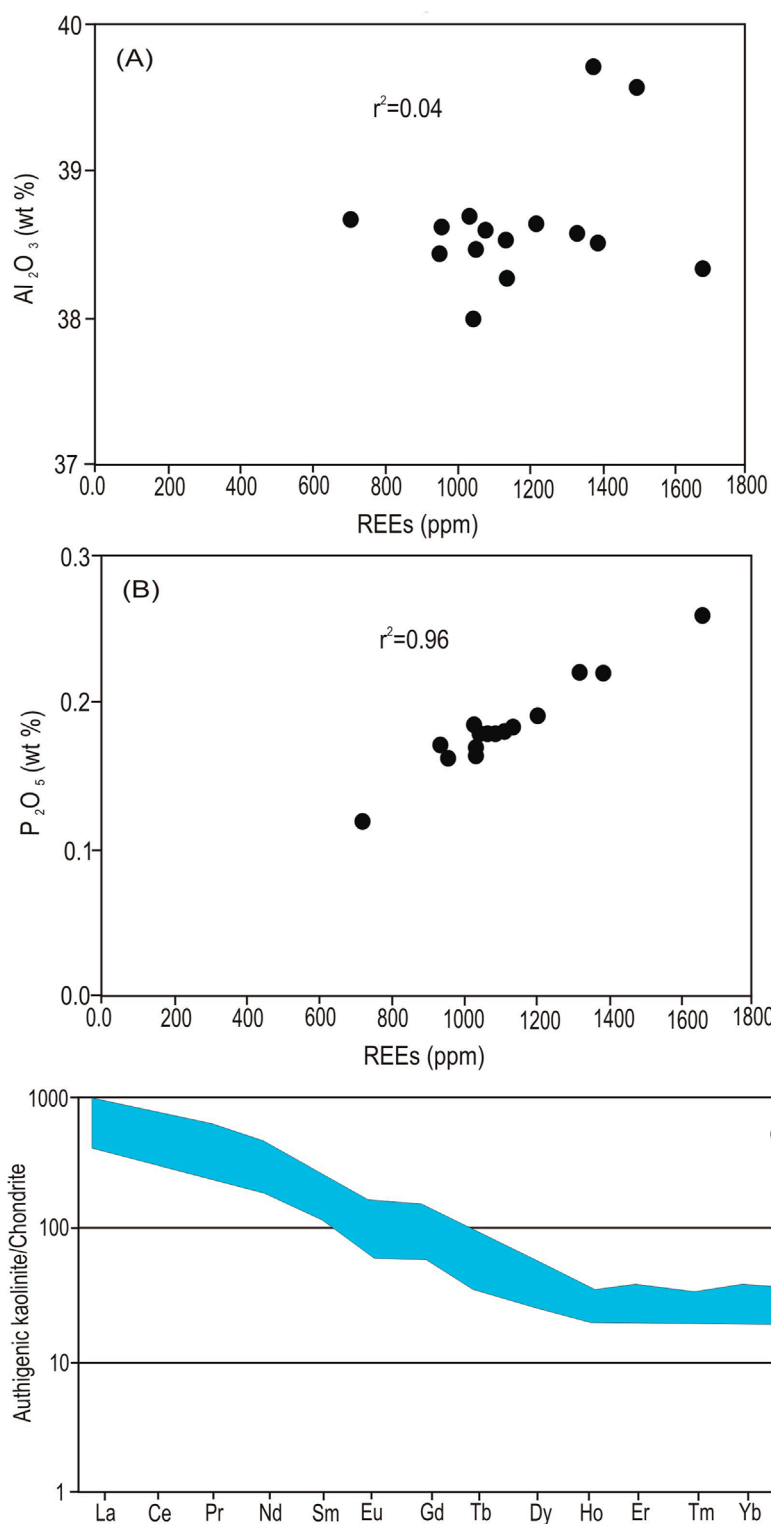
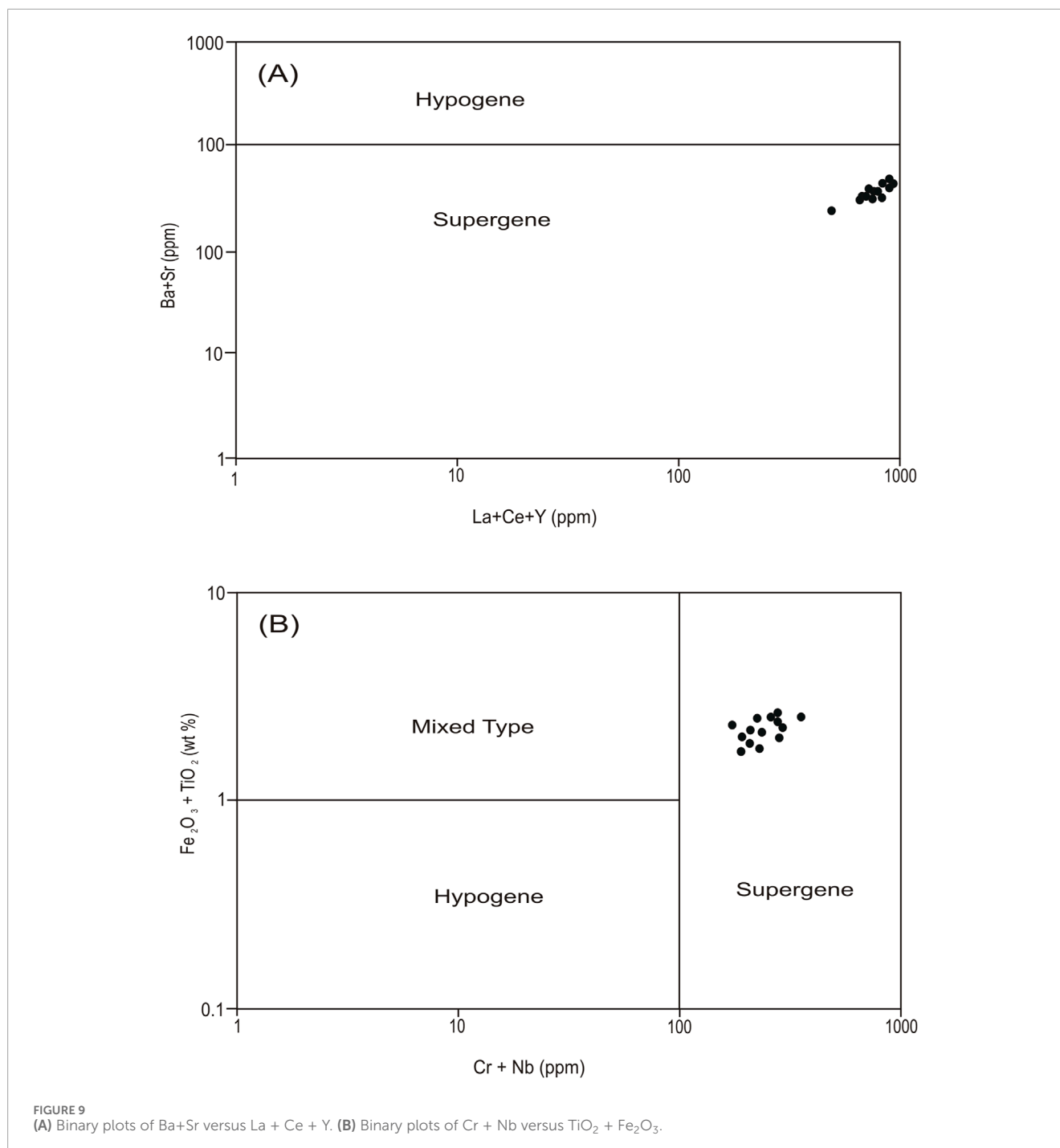


FIGURE 8
(A) Σ REEs did not correlate with Al_2O_3 . **(B)** REEs correlate positively with P_2O_5 . **(C)** Chondrite-normalized REE patterns of the authigenic kaolinite.

applications and can help assess the economic value of kaolin. Kaolinite is used in different industrial applications, such as the ceramic, paper, abrasive, paint, and plastic industries (Nouri and Masoumi, 2020). The major oxide content of the authigenic kaolinite

from the Biyahd Formation was compared to that of Georgia kaolin in the United States (Murray and Keller, 1993), Cornwall kaolin (SKD) (Harben, 1999), Cornwall kaolin (ECC) (Bloodworth et al., 1993), as well as its application in paper filling, paper coating,



ceramics (Siddiqui et al., 2005), and cosmetics and pharmaceuticals (Lopez-Galindo et al., 2007) (Figures 10A, B). The geochemical properties of the studied kaolinite show that the authigenic kaolinite from the Biyadh Formation is suitable for use in the paper coating and filler industries. As a filler, its function is related to the internal network of the paper, while as a coating, it improves the surficial characteristics of paper, including brightness, glossiness, smoothness, and ink (Bundy, and Ishley, 1991; Murray, 2006; Murray and Kogel, 2005). However, the use of kaolin in the paper industry is dependent on the particle size. SEM of the studied kaolinite indicated that the kaolinite occurs in a homogeneous size

and that particles greater than 10 μm are dominant (Figure 4C). Therefore, the studied kaolinite is recommended for use in coating and filler applications. Kaolinite constitutes an average of 25 wt% in earthenware, 60 wt% in porcelain, 20 wt%–30 wt% in vitreous-China sanitary ware, and 20 wt% in electrical porcelain and wall tiles (Jepson, 1984). In general, the kaolin used in ceramic industries needs high Al_2O_3 content. Products such as super-standard porcelain and sanitary ware should have high alumina contents, and therefore, only kaolinite with high Al_2O_3 is used as a raw material for these industries. On the other hand, the silica content of this raw material should be less than 50 wt%

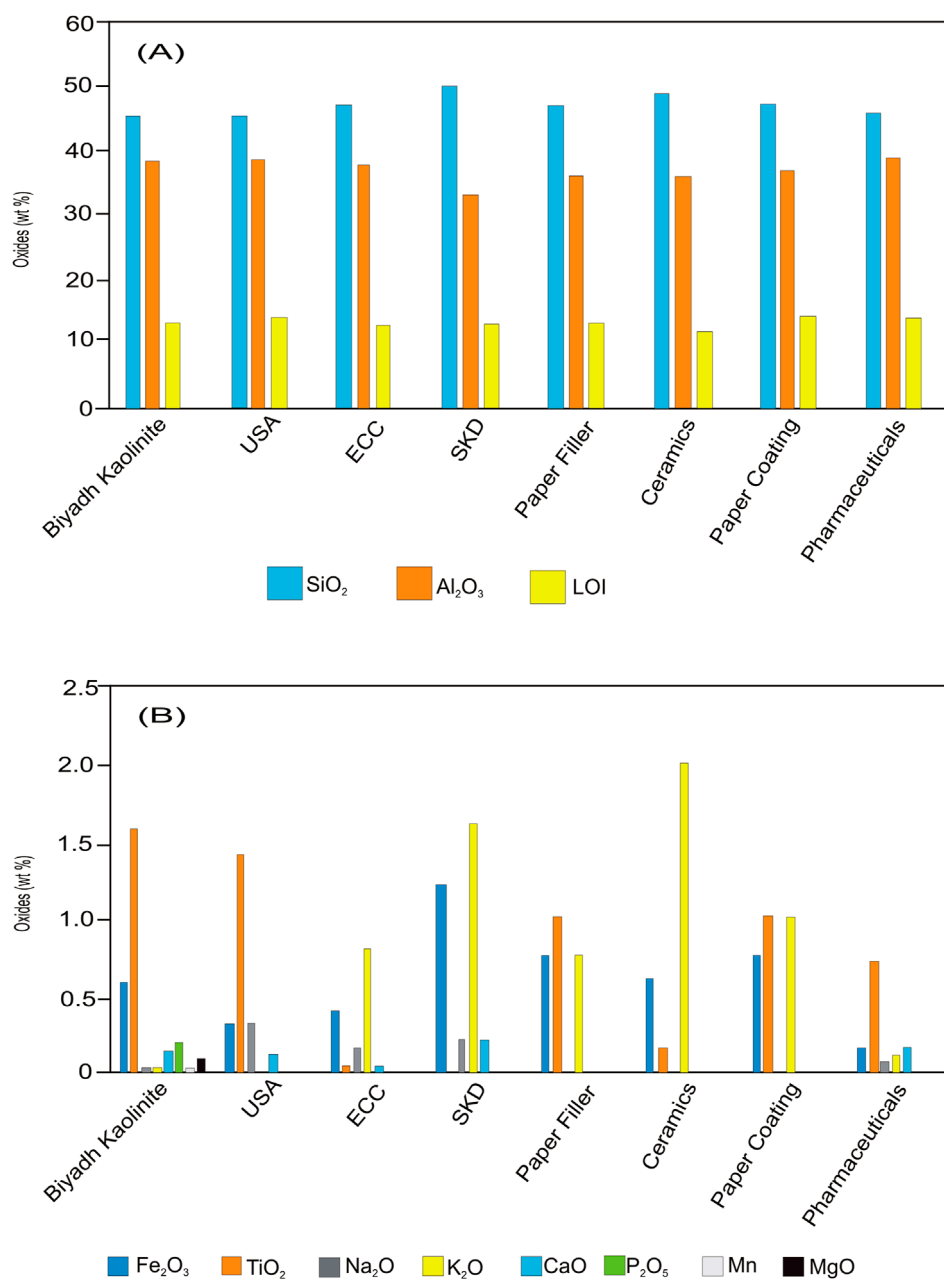


FIGURE 10 Comparison between the geochemical parameters of the authigenic kaolinite from the Biyadh Formation and the standard parameters of various industrial applications of kaolinite. (A) Major components. (B) Minor oxides.

in super-standard porcelain and sanitary ware products (Nouri and Masoumi, 2020). The authigenic kaolinite from the Biyadh Formation is characterized by high Al₂O₃ (>38wt%) and less than 50wt% SiO₂, which indicates that this kaolinite can be exploited for super-standard porcelain and sanitary ware. Ti and Fe are the main impurities in kaolin deposits and play an important role in determining the quality of kaolin and industrial utilization. These two elements affect the whiteness of kaolin and negatively influence the transparency of the products, reducing the use of kaolin and limiting its application in certain industries (Calderon et al., 2005). The Fe and Ti concentrations in the studied kaolinite are low

compared to those in the standard references; therefore, neither Fe nor Ti will affect the transparency of the products from this kaolinite. Regarding pharmaceuticals and cosmetics, the studied kaolinite has slightly higher Ti contents (1.6 wt%) than the TiO₂ range in the kaolinite for the pharmaceutical and cosmetics industries (0.0–1.4 wt%) (Lopez-Galindo et al., 2007). Partial removal of TiO₂ from this kaolinite during its processing and separation will allow its application in the pharmaceutical and cosmetics industries.

White sands of the Biyadh Formation are exploited as a raw material for glass industries. The Al₂O₃ contents in some of these sands range from 1.1 wt% to 6.2 wt% (Al-Harbi et al.,

1995), sourced mainly from the authigenic kaolinite in these sands. Alumina impurities may alter the clarity and color of glass. For glass manufacturing, the Al_2O_3 content in the raw silica sand should be kept low, typically less than 0.5 wt% Al_2O_3 (Edem et al., 2014; Ushie et al., 2005). Therefore, the separation of kaolinite from these deposits will enhance the physico-chemical characteristics of these sands in addition to the economic value of the separated kaolinite itself.

5.3.2 Possible source of REEs as by-product

The demand for REEs has significantly increased, and less conventional resources of REEs are being explored for economic feasibility. Over the past years, four primary types of deposits have been identified as significant sources of REEs (Van Gosen et al., 2014). These deposits include carbonatites, alkaline igneous rocks, ion-adsorption clays, and monazite-xenotime-bearing placer deposits (Van Gosen et al., 2014). Recent studies, however, suggest the potential of REE extraction from alternative sources such as coal, ocean water, and regoliths linked with coastal plain clays (Drost and Wang, 2016; Foley and Ayuso, 2015; Rozelle et al., 2016). Gardner (2016) studied the REE content of Georgian kaolins and evaluated the exploration potentials of this deposit. He found some REE-bearing minerals, such as monazite and zircon, which contain a considerable amount of REEs.

The authigenic kaolinite separated from the Biyahd Formation shows exceptionally high REE contents, indicating its potential as a secondary source of REEs during kaolinite separation and processing. This study also shows that these REEs are associated with a phosphate phase. The occurrence of REEs as phosphate phases is widely demonstrated in the literature on kaolinization processes (Baoumy, 2014; Dill et al., 1995a; Dill et al., 1995b). This phase is soluble in hydrochloric acid, nitric acid, and alcohol (Tanaka et al., 2010), which makes the extraction of these elements an easy and cheap process. Additionally, other trace elements of economic importance that occur in relatively high concentrations, such as Zr, can be separated from the studied kaolinite. Although Li occurs in concentrations lower than the lowest industrial limit of Li in ores, it still has considerably high contents in the studied kaolinite, which can be considered a possible source of Li in the future.

6 Conclusion

Globally, the formation of authigenic kaolinite interested researchers due to its effect on the sandstone reservoir properties regardless of its potential industrial applications. It is also assumed that this kaolinite was sourced from feldspars without evidence. The first detailed geochemical and mineralogical investigations on the authigenic kaolinite from the Lower Cretaceous white sandstones from the Biyahd Formation, Saudi Arabia, revealed the following findings:

- Kaolinite occurs as blocky, pore-filling cement formed of euhedral, pseudo-hexagonal plates, which, along with its HI, indicates its authigenic origin during the late stages of diagenesis during subaerial exposure and/or at shallow burial depths of the host sandstones due to the influx of meteoric water.
- Anatase, the main impurity in the separated kaolinite, exists as very fine grains (micro to nano-sized) between the kaolinite flakes.

- The elevated concentrations of REEs, Zr, Ti, and Li suggest a possible enrichment of these elements during the diagenesis of the studied kaolinite.
- Geochemical and mineralogical properties suggest the potential application of the studied kaolinite in paper coating and filler as well as in super-standard porcelain and sanitary ware.
- Removal of TiO_2 from this kaolinite will allow its application in the pharmaceutical and cosmetics industries.
- The results of this study added a new resource of the strategic REEs, which have many industrial applications.

Data availability statement

The original contributions presented in the study are included in the article/supplementary material, further inquiries can be directed to the corresponding author.

Author contributions

AA: Investigation and Writing – original draft. AQ: Investigation and Writing – original draft. MSA: Investigation, Writing – original draft, and Writing – review and editing. AMA: Investigation, Project administration, Writing – original draft, and Writing – review and editing. HB: Data curation, Formal analysis, Validation, and Writing – original draft. MMA: Formal analysis, Investigation, and Writing – review and editing. AB: Formal analysis, Investigation, and Writing – review and editing. MF: Formal analysis, Visualization, and Writing – review and editing. SA: Formal analysis, Visualization, and Writing – review and editing.

Funding

The author(s) declare that financial support was received for the research and/or publication of this article. This work was funded by KACST.

Acknowledgments

The authors are grateful for the King Abdulaziz City for Science and Technology (KACST) for supporting this work.

Conflict of interest

Author HB was employed by Arabian Geophysical and Surveying Co. (ARGAS).

The remaining authors declare that the research was conducted in the absence of any commercial or financial relationships that could be construed as a potential conflict of interest.

Generative AI statement

The author(s) declare that no Generative AI was used in the creation of this manuscript.

Publisher's note

All claims expressed in this article are solely those of the authors and do not necessarily represent those of their affiliated

organizations, or those of the publisher, the editors and the reviewers. Any product that may be evaluated in this article, or claim that may be made by its manufacturer, is not guaranteed or endorsed by the publisher.

References

- Al-Abady, A. (2022). Characterization and potential upgrading of el-zaafarana white sand by attrition scrubbing. *J. Univ. Shanghai Sci. Technol.* 24 (4), 79–90. doi:10.51201/JUSST/22/0345
- Alali, J. M. (2020). Beneficiation of white kaolinitic sandstone to produce kaolin concentrate from Wadi Siq-Rakya Area in Wadi Araba, Jordan. *Open J. Geol.* 10, 829–850. doi:10.4236/ojg.2020.108037
- Al-Harbi, O., Amjad, M., Alabdulaaly, A., Khater, G., and Alsari, A. (1995). Evaluation of white silica sand in Al-Kharj area for industrial applications. *4th Saudi Int. Conf. II*, 307–311. doi:10.4197/Eng.15-2.8
- Alharbi, T. (2023). Assessment of the Biyadh groundwater quality and geochemical process in Saudi Arabia using statistical, modelling, and WQI methods. *J. King Saud University-Science* 35, 102847. doi:10.1016/j.jksus.2023.102847
- Anjos, S. M. C., De Ros, L. F., De Souza, R. S., De Assis Silva, C. M., and Sombra, C. L. (2000). Depositional and diagenetic controls on the reservoir quality of Lower Cretaceous Penedencia sandstones, Potiguar rift basin. *Braz. AAPG Bull.* 84, 1719–1742. doi:10.1306/8626C375-173B-11D7-8645000102C1865D
- Araújo, F. R., Baptista, J. G., Marcal, L., Ciuffia, K. J., Nassara, E. J., Calefi, P. S., et al. (2014). Versatile heterogeneous dipicolinate complexes grafted into kaolinite: catalytic oxidation of hydrocarbons and degradation of dyes. *Catal. Today* 227, 105–115. doi:10.1016/j.cattod.2013.09.031
- Arditto, P. A. (1983). Mineral-groundwater interactions and the formation of authigenic kaolinite within the southeastern intake beds of the Great Australian (Artesian) Basin, New South Wales, Australia. *Sediment. Geol.* 35, 249–261. doi:10.1016/0037-0738(83)90061-1
- Baioumy, H. (2014). Geochemistry and origin of the Cretaceous sedimentary kaolin deposits, Red Sea, Egypt. *Chem. Erde - Geochem.* 74 (2), 195–203. doi:10.1016/j.chemer.2013.06.008
- Baioumy, H., Farahat, M., Arifin, M. H., Anuar, A., and Al-Kahtany, K. (2021). Hypogene kaolin deposits from felsic intrusive rocks (Peninsular Malaysia) with special reference to rare earth elements and stable isotopes geochemistry. *Geosciences J.* 1226–4806. doi:10.1007/s12303-021-0003-9
- Baioumy, H., Gilg, H. A., and Taubald, H. (2012). Mineralogy and geochemistry of the sedimentary kaolin deposits from Sinai, Egypt: implications for control by the source rocks. *Clays Clay Minerals* 60, 633–654. doi:10.1346/ccmn.2012.0600608
- Bandel, K., Kuss, J., and Malchus, N. (1987). The sediments of wadi qena (eastern desert, Egypt). *J. Afr. Earth Sci.* 6, 427–455. doi:10.1016/0899-5362(87)90086-8
- Beall, A. O., and Squyres, C. H. (1980). Modern frontier exploration strategy, a case history from upper Egypt. *Oil Gas J.* 4, 106–110. doi:10.1306/C1EA56A2-16C9-11D7-8645000102C1865D
- Berger, G., Lachapagne, J. C., Velde, B., Beaufort, D., and Lanson, B. (1997). Kinetic constraints on illitization reactions and the effects of organic diagenesis in sandstone/shale sequences. *Appl. Geochem.* 12, 23–35. doi:10.1016/s0883-2927(96)00051-0
- Bizaia, N., De Faria, E. H., Ricci, G. P., Calefi, P. S., Nassara, E. J., Castro, K. A. D. E., et al. (2009). Porphyrin-kaolinite as efficient catalyst for oxidation reactions. *ACS Appl. Mater. Interfaces* 1, 2667–2678. doi:10.1021/am900556b
- Bjørlykke, K., and Jahren, J. (2012). Open or closed geochemical systems during diagenesis in sedimentary basins: constraints on mass transfer during diagenesis and the prediction of porosity in sandstone and carbonate reservoirs. *AAPG Bull.* 96, 2193–2214. doi:10.1306/04301211139
- Bloodworth, A. J., Highley, D. E., and Mitchell, C. J. (1993). *Industrial minerals laboratory manual: kaolin*, 76. BGS Technical Report WG/93/1.
- Boukhamsin, H., Peyrot, D., Lang, S., and Vecoli, M. (2023). Low-latitude? upper Barremian-lower Aptian palynoflora and paleovegetation of the Biyadh Formation (Arabian Plate, eastern margin of northern Gondwana): evidence for a possible cold snap. *Cretac. Res.* 129, 104995. doi:10.1016/j.cretres.2021.104995
- Boynton, W. V. (1984). "Geochemistry of the REE: meteorite studies," in *Rare earth element geochemistry*. Editor P. Henderson (Amsterdam: Elsevier), 63–114.
- Bundy, W. M., and Ishley, J. N. (1991). Kaolin in paper filling and coating. *Appl. Clay Sci.* 5 (5–6), 397–420. doi:10.1016/0169-1317(91)90015-2
- Calderon, G. D. T., Rodriguez, J. I., Ortiz-Mendez, and Torres-Martinez, L. M. (2005). Iron leaching of a Mexican clay of industrial interest by oxalic acid. *J. Mater.* 1, 1–8. doi:10.2240/azojomo0168
- Chen, B., Wang, F., Shi, J., Chen, F., and Shi, H. (2019). Origin and sources of minerals and their impact on the hydrocarbon reservoir quality of the Paleogene Lulehe Formation in the eboliang area, northern qaidam basin, China. *Minerals* 9, 436. doi:10.3390/min9070436
- Chuhan, F., Bjørlykke, K., and Lowrey, C. J. (2001). Closed-system burial diagenesis in reservoir sandstones: example from the Garn Formation at Haltenbanken area, offshore Mid-Norway. *J. Sediment. Res.* 71, 15–26. doi:10.1306/041100710015
- Curtis, C. D. (1983). Geochemistry of porosity reduction and enhancement in clastic sediments. In: *Petroleum geochemistry and exploration of Europe* (Ed J. Brooks), Blackwell, Oxford, pp. 113–125.
- Daou, I., Lecomte-Nana, G. L., Tessier-Doyen, N., Peyratout, C., Gonon, M. F., and Guinebreiere, R. (2020). Probing the dehydroxylation of kaolinite and halloysite by *in situ* high temperature X-ray diffraction. *Minerals* 10, 480. doi:10.3390/min10050480
- Dezso, G. K., and Detellier, C. (2014). Intercalation of two phenolic acids in an ionic liquid-kaolinite nanohybrid material and desorption studies. *Appl. Clay Sci.* 97–98, 153–159. doi:10.1016/j.clay.2014.04.038
- De Faria, E. H., Ricci, G. P., Marçal, L., Nassara, E. J., Vicent, e M. A., Trujillano, R., et al. (2012). Green and selective oxidation reactions catalyzed by kaolinite covalently grafted with Fe(III) pyridine-carboxylate complexes. *Catal. Today* 187, 135–149. doi:10.1016/j.cattod.2011.11.029
- Dill, H. G., Bosse, H. R., Henning, H., Fricke, A., and Ahrendt, H. (1997). Mineralogical and chemical variations in hypogene and supergene kaolin deposits in a mobile fold belt the Central Andes of northwestern Peru. *Miner. Deposita* 32, 149–163. doi:10.1007/s001260050081
- Dill, H. G., Bosse, H. R., and Kassbohm, J. (2000). Mineralogical and chemical studies of volcanic-related argillaceous industrial minerals of the central American cordillera (western El Salvador). *Econ. Geol.* 95, 517–538. doi:10.2113/gsecongeo.95.3.517
- Dill, H. G., Buzatu, A., Kleyer, C., Balaban, S. I., Pöllmann, H., and Füssel, M. (2022). A composite terrain-and-provenance analysis tied to specific times of a basement-foreland drainage system and its gravel-sand-clay deposits (Bohemian Massif, SE Germany). *Sediment. Geol.* 441, 106266. doi:10.1016/j.sedgeo.2022.106266
- Dill, H. G., Fricke, A., and Henning, K. H. (1995a). The origin of Ba- and REE-bearing aluminium-phosphate-sulphate minerals from the Lohrheim kaolinitic clay deposit (Rheinisches Schiefergebirge, Germany). *Appl. Clay Sci.* 10 (3), 231–245. doi:10.1016/0169-1317(95)00023-w
- Dill, H. G., Fricke, A., Henning, K. H., and Theune, C. H. (1995b). Aluminium phosphate mineralization from the hypogene La Vanguardia kaolin deposit (Chile). *Clay Miner.* 30 (3), 249–256. doi:10.1180/claymin.1995.030.3.08
- Dill, H. G., Kaufhold, S., Ehling, A., and Bowitz, J. (2016). Oxidized and reduced kaolin fan deposits: their sedimentological-mineralogical facies and physical-chemical regime (North-Bavarian Kaolin Mining District, Germany). *Ore Geol. Rev.* 72, 459–484. doi:10.1016/j.oregeorev.2015.08.003
- Dill, H. G., Kus, J., Abed, A. M., Sachsenhofer, R. F., and Khair, H. A. (2009). Diagenetic and epigenetic alteration of Cretaceous to Paleogene organic-rich sedimentary successions in northwestern Jordan, typical of the western margin of the Arabian Plate. *GeoArabia* 14 (2), 101–140. doi:10.2113/geoarabia1402101
- Drost, D., and Wang, R. (2016). "Rare earth element criticality and sustainable management," in 4th International Conference on Sensors, Measurement and Intelligent Materials (ICSMIM 2015), 914–919.
- Edem, C. A., Malu, S. P., and Ita, B. I. (2014). Characterization and beneficiation of the glass making potentials of silica sand deposit from river benue north Central Nigeria. *J. Nat. Sci. Res.* 4 (19), 49–58.
- El Sayed, M. A., Fathy, W. M., Salleh, A. M., Ibrahim, S. S., and Moharam, M. R. (2018). Processing of Wadi Qena kaolinitic white sands by selective dispersion and leaching for industrial uses. *J. Al-Azhar Univ. Eng. Sect.* 13 (47), 530–545. doi:10.21608/aej.2018.19059
- El-Wekeil, S. S., and Gaafar, F. S. (2014). Characterization and economic potential of the white sandstones of the naqus Formation in wadi qena, northern eastern desert, Egypt. *Middle East J. Appl. Sci.* 4, 392–408.
- Fan, A., Yang, R., Lenhardt, N., Wang, M., Han, Z., Li, J., et al. (2019). Cementation and porosity evolution of tight sandstone reservoirs in the Permian Sulige gas field, Ordos Basin (central China). *Mar. Petroleum Geol.* 103, 276–293. doi:10.1016/j.marpetgeo.2019.02.010

- Fan, G., Xu, G., Shi, A., Smith, M. P., Kynicky, J., and Wei, C. (2023). Origin of heavy rare earth elements in highly fractionated peraluminous Granites. *Geochimica Cosmochimica Acta* 343, 371–383. doi:10.1016/j.gca.2022.12.019
- Foley, N., and Ayuso, R. (2015). REE enrichment in granite derived regolith deposits of the Southeastern United States: prospective source rocks and accumulation processes. *B. C. Geol. Surv. Pap.* 3, 131138.
- Galan, E., Aparicio, P., Gonzales, I., and Laiglesia, A. (1994). Influence of associated components of kaolin on the degree of disorder of kaolinite as determined by XRD. *Geol. Carpathica Clays* 45, 59–75.
- Gao, J., Ma, B., Lu, Y., Zhang, W., and Cao, Q. (2022). Origin of authigenic kaolinite with implications for Permian tight gas sandstone reservoirs in the northern Ordos Basin, central China. *J. Nat. Gas Sci. Eng.* 99, 104429. doi:10.1016/j.jngse.2022.104429
- Gardner, D. J. (2016). *A study of mineral impurities within the Georgia Kaolins: unpublished MS thesis*. Atlanta, Georgia, USA: Georgia State University, 80. Available online at: http://scholarworks.gsu.edu/geosciences_theses/101.
- Harben, W. P. (1999). The industrial mineral handbook III. A guide to markets, specification and prices. *Int. Miner. Inf. Ltd.*, 106–112. doi:10.4236/msce.2021.93002
- Hinckley, D. (1963). “Variability in crystallinity values among the kaolin deposits of the Coastal Plain of Georgia and South Carolina,” in Proceedings of the 11th International Conference of Clays and Clay Minerals, 229–235.
- Höhn, S., Frimmel, H. E., and Pašava, J. (2014). The rare earth element potential of kaolin deposits in the Bohemian Massif (Czech Republic, Austria). *Min. Deposita*. doi:10.1007/s00126-014-0542-3
- Howari, F. (2015). Evaluation of chemical and petrographic characteristics of silica sand from tabuk in Saudi Arabia. *J. Geol. Geosciences* 4 (3), 1–8. doi:10.4172/2329-6755.1000200
- Ibrahim, S. S., Fathy, W. M., Elsayed, M. A., Saleh, A. M., Boulos, T. R., and Moharam, M. R. (2018). An Egyptian sandstone deposit as a source of good quality kaolin and ultra-pure silica sand: sample characterization and separation (Part I). *Glob. J. Res. Eng. Industrial Eng.* 18 (1), 21–30. doi:10.17406/GJREGVOL18IS1PG21
- Jenner, G. A., Longerich, H. P., Jackson, S. E., and Fryer, B. J. (1990). ICP-MS-A powerful tool for high-precision trace-element analysis in Earth sciences: evidence from analysis of selected U.S.G.S. reference samples. *Chem. Geol.* 83 (1-2), 133–148. doi:10.1016/0009-2541(90)90145-w
- Jepson, W. B. (1984). Kaolins: their properties and uses. *Philosophical Trans. R. Soc. A Math. Phys. Eng. Sci.* 311 (1517), 411–432. doi:10.1098/rsta.1984.0037
- Keller, M., Bohnsack, D., Koch, R., Hinderer, M., Hornung, J., Al Ajmi, H., et al. (2019). “Outcrop analog studies of the wasia-biyadh and aruma aquifers in the kingdom of Saudi Arabia,” in *Siliciclastic reservoirs of the Arabian plate*. Editors H. R. AlAnzi, R. A. Rahmani, R. J. Steel, and O. M. Soliman (United States: AAPG Memoir), 116, 317–382.
- Kleeberg, R., and Bergmann, J. (1998). “Quantitative Röntgenphasenanalyse mit den Rietveld-Programmen BGMN und AUTOQUANT in der täglichen Laborpraxis,” in *Tone in der Geotechnik und Baupraxis*. Editors K. H. Henning, and J. Kasbohm (Germany: Beitrage zur Jahrestagung Greifswald, Berichte der DTTG, Greifswald), 237–250.
- Lanson, B., Beaufort, D., Berger, G., Bauer, A., Cassagnabere, A., and Meunier, A. (2002). Authigenic kaolin and illitic minerals during burial diagenesis of sandstones: a review. *Clay Miner.* 37 (1), 1–22. doi:10.1180/0009855023710014
- Le Nindre, Y., Davies, R. B., Benoit, I., Krystynd, L., Vaslete, D., Bruno Vrielynck, B., et al. (2023). The Middle to Late Triassic of Central Saudi Arabia with emphasis on the Jilh Formation. Part II: sequence stratigraphy, depositional and structural history, correlations, and paleogeography. *Géoscience-Sciences la Planète* 355 (S2), 99–135. doi:10.5802/crgeos.217
- Le Nindre, Y., Vaslet, D., Maddah, S. S., and Al-Husseini, M. I. (2008). Stratigraphy of the valanginian? To early paleocene succession in central Saudi Arabia outcrops: implications for regional arabian sequence stratigraphy. *GeoArabia* 13 (2), 51–86. doi:10.2113/geoarabia130251
- Li, S., Lee, J.-H., Hwang, S. M., and Kim, Y.-J. (2023). Reversible flowering of CuO nanoclusters via conversion reaction for dual-ion Li metal batteries. *Nano Converge* 10, 4. doi:10.1186/s40580-022-00353-3
- Lopez-Galindo, A., Viseras, C., and Cerezo, P. (2007). Compositional, technical and safety specifications of clays to be used as pharmaceutical and cosmetic products. *Appl. Clay Sci.* 36, 51–63. doi:10.1016/j.clay.2006.06.016
- Ma, B., Cao, Y., Eriksson, K., Jia, Y., and Gill, B. (2017). Depositional and diagenetic controls on deeply-buried Eocene sublacustrine fan reservoirs in the Dongying depression, Bohai Bay basin, China. *Mar. Petroleum Geol.* 82, 297–317. doi:10.1016/j.marpetgeo.2017.02.014
- Ma, B., Cao, Y., Zhang, Y., and Eriksson, K. A. (2020). Role of CO₂-water-rock interactions and implications for CO₂ sequestration in Eocene deeply buried sandstones in the Bonan Sag, eastern Bohai Bay Basin, China. *Chem. Geol.* 541, 119585. doi:10.1016/j.chemgeo.2020.119585
- Ma, B., Eriksson, K. A., Cao, Y., Jia, Y., Wang, Y., and Gill, B. C. (2016). Fluid flow and related diagenetic processes in a rift basin: evidence from the fourth member of the Eocene Shahejie Formation interval, Dongying depression, Bohai Bay Basin, China. *AAPG Bull.* 100, 1633–1662. doi:10.1306/04211615207
- Ma, B., Lu, Y., Eriksson, K. A., Peng, L., Xing, F., and Li, X. (2021). Multiple organic-inorganic interactions and influences on heterogeneous carbonate-cementation patterns: example from Silurian deeply buried sandstones, central Tarim Basin, north-western China. *Sedimentology* 68, 670–696. doi:10.1111/sed.12797
- Mahmoud, E. R. I., Shaharoun, A. M., Aljabri, A., Almohamadi, H., and Mohammed Farhan, M. (2022). Assessment of sand and glass industry in Saudi Arabia. *Sustainability* 14, 12904. doi:10.3390/su141912904
- Maiza, P. J., Pieroni, D., and Marfil, S. A. (2003). “Geochemistry of hydrothermal kaolins in the SE area of Los Menucos, province of Río Negro, Argentina,” in 2001, *A clay odyssey*. Editors E. A. Dominguez, G. R. Mas, and F. Cravero (Amsterdam: Elsevier), 123–130.
- Mansurbeg, H., Morad, S., Salem, A., Marfil, R., El-ghali, M. A. K., Nystuen, J. P., et al. (2008). Diagenesis and reservoir quality evolution of Palaeocene deep-water, marine sandstones, the Shetland-Faroes Basin, British continental shelf. *Mar. Petroleum Geol.* 25, 514–543. doi:10.1016/j.marpetgeo.2007.07.012
- Marfil, R., Delgado, A., Rossi, C., La Iglesia, A., and Ramseyer, K. (2003). Origin and diagenetic evolution of kaolin in reservoir sandstones and associated shales of the Jurassic and Cretaceous, Salam Field, Western Desert (Egypt). *Int. Assoc. Sedimentol. Spec. Publ.* 34, 319–342. doi:10.1002/9781444304336.ch14
- Matusik, J., and Bajda, T. (2013). Immobilization and reduction of hexavalent chromium in the interlayer space of positively charged kaolinites. *J. Colloid Interface Sci.* 398, 74–81. doi:10.1016/j.jcis.2013.02.015
- Matusik, J., and Matykowska, L. (2014). Behaviour of kaolinite intercalation compounds with selected ammonium salts in aqueous chromate and arsenate solutions. *J. Mol. Struct.* 1071, 52–59. doi:10.1016/j.molstruc.2014.04.063
- Meng, W., Niu, Z., Hu, Y., An, T., Liu, K., and Qiang, G. (2020). Genesis of authigenic kaolinite and its indicative significance to secondary pores in petroliferous basins: a case study in the Dongying Sag, Bohai Bay Basin, Eastern China. *J. Petroleum Sci. Eng.* 186, 106698. doi:10.1016/j.petrol.2019.106698
- Moore, M. D., and Reynolds, R. C., Jr. (1989). *X-Ray diffraction and the identification and analysis of clay minerals*. Oxford, New York: Oxford University Press, 332.
- Morad, S., Al-Ramadan, K., Ketzner, J. M., and De Ros, L. F. (2010). The impact of diagenesis on the heterogeneity of sandstone reservoirs: a review of the role of depositional facies and sequence stratigraphy. *AAPG Bull.* 94, 1267–1309. doi:10.1306/04211009178
- Moshrif, M. A. (1980). Recognition of fluvial environment in the Biyadh-Wasia sandstones (lower-middle Cretaceous) as revealed by textural analysis. *J. Sediment. Petrology* 50, 603–612. doi:10.1306/212F7A5E-2B24-11D7-8648000102C1865D
- Murray, H. H. (2006). Kaolin applications. *Dev. Clay Sci.* 2, 85–109. doi:10.1016/S1572-4352(06)02005-8
- Murray, H. H., and Keller, W. D. (1993). “Kaolin, kaolin, and kaolin,” in *Kaolin genesis and utilization*. Editors H. H. Murray, W. Bondy, and C. Harvey (Aurora, USA: Special Publication N°1, The Clay Mineral Society), 1–24.
- Murray, H. H., and Kogel, J. E. (2005). Engineered clay products for the paper industry. *Appl. Clay Sci.* 29 (3-4), 199–206. doi:10.1016/j.clay.2004.12.005
- Nakagaki, S., Machado, G. S., Halma, M., dos Santos Marangon, A. A., de Freitas Castro, K. A. D., Mattoso, N., et al. (2006). Immobilization of iron porphyrins in tubular kaolinite obtained by an intercalation/delamination procedure. *J. Catal.* 242, 110–117. doi:10.1016/j.jcat.2006.06.003
- Nikdel, M., Tafti, M. G., and Nikdel, M. (2024). Discovery and primary study of the lithium content in the karst-type bauxite deposit, Jajarm, Iran. *Carbonates Evaporites* 39 (2), 25. doi:10.1007/s13146-024-00941-w
- Nouri, T., and Masoumi, R. (2020). Geochemical and industrial properties of the Kejal kaolin deposit, NW Iran. *Turkish J. Earth Sci.* 29 (2), 325–346. doi:10.3906/yer-1906-7
- Platiasa, S., Vatalisa, K. I., and Charalampides, G. (2014). Suitability of quartz sands for different industrial applications. *Int. Conf. Appl. Econ. (ICOAE) 2014 Procedia Econ. Finance* 14, 491–498. doi:10.1016/s2212-5671(14)00738-2
- Powell, J. (1989). Stratigraphy and sedimentation of the phanerozoic rocks in central and south Jordan. *Nat. Resour. Auth. Bull. Amman* 11, 72.
- Powers, R. W., Ramirez, L. F., Redmond, C. D., and Elberg, E. L. (1966). *Geology of the arabian peninsula*, 560. Geological Survey Professional Paper, USGS, 1–147.
- Rozelle, P. L., Khadilkar, A. B., Pulati, N., Soundarajan, N., Klima, M. S., Mosser, M. M., et al. (2016). A study on removal of rare-earth elements from US coal byproducts by ion exchange. *Metallurgical Mater. Trans.* 3, 6–17. doi:10.1007/s40553-015-0064-7
- Siddiqui, M. A., Ahmed, Z., and Saleemi, A. A. (2005). Evaluation of Swat kaolin deposits of Pakistan for industrial uses. *Appl. Clay Sci.* 29, 55–72. doi:10.1016/j.clay.2004.09.005
- Steineke, M., Bramkamp, R. A., and Sander, N. J. (1958). *Stratigraphic relations of arabian jurassic oil*. Tulsa, USA: American Association of Petroleum Geologists Symposium, 1294–1329.
- Stoffregen, R. E., and Alpers, C. N. (1987). Woodhouseite and svanbergite in hydrothermal ore deposits: products of apatite destruction during advanced argillite alteration. *J. Mineralogical Assoc. Can.* 25, 201–211.

- Surdam, R. C., Boese, S. W., and Crossey, L. J. (1984). The chemistry of secondary porosity. In: *Clastic diagenesis* (Eds D. A. McDonald, and R. C. Surdam). United States: AAPG Memoir 37, 127–149.
- Tabelin, B., Dallas, J., Casanova, S., Pelech, T., Bournival, G., Saydam, S., et al. (2021). Towards a low-carbon society: a review of lithium resource availability, challenges and innovations in mining, extraction and recycling, and future perspectives. *Miner. Eng.* 163, 106743. doi:10.1016/j.mineng.2020.106743
- Tanaka, Y., Kojima, T., Takata, Y., Chainani, A., Lovesey, S. W., Knight, K. S., et al. (2010). Determination of structural chirality of berlinite and quartz using resonant X-ray diffraction with circularly polarized X-rays. *Phys. Rev. B* 81 (14), 144104. doi:10.1103/physrevb.81.144104
- Taylor, T. R., Giles, M. R., Hathon, L. A., Diggs, T. N., Braunsdorf, N. R., Birbiglia, G. V., et al. (2010). Sandstone diagenesis and reservoir quality prediction: models, myths, and reality. *AAPG Bull.* 94, 1093–1132. doi:10.1306/04211009123
- Tonlé, I. K., Letaief, S., Ngameni, E., Walcarius, A., and Detellier, C. (2011). Square wave voltammetric determination of lead (II) ions using a carbon paste electrode modified by a thiol-functionalized kaolinite. *Electroanalysis* 23, 245–252. doi:10.1002/elan.201000467
- Ushie, F. A., Esu, E., and Udom, G. J. (2005). A preliminary evaluation of Otamiri River sands for the production of plain glass. *J. Appl. Sci. Environ. Manag.* 9 (1), 65–68.
- Van Gosen, B. S., Verplanck, P. L., Long, K. R., Gambogi, J., and Seal, R. R. (2014). The rare-earth elements: vital to modern technologies and lifestyles. *US Geol. Survey*, 2014–3078. doi:10.3133/fs20143078
- Van Keer, I., Muchez, P., and Viaene, W. (1998). Clay mineralogical variations and evolutions in sandstone sequences near a coal seam and shales in the Westphalian of the Campine Basin (NE Belgium). *Clay Miner.* 33, 159–169. doi:10.1180/000985598545345
- Waldmann, S., and Gaupp, R. (2016). Grain-rimming kaolinite in Permian Rotliegend reservoir rocks. *Sediment. Geol.* 335, 17–33. doi:10.1016/j.sedgeo.2016.01.016
- Wanas, H. A. (2011). The Lower Paleozoic rock units in Egypt: an overview. *Geosci. Front.* 2 (4), 491–507. doi:10.1016/j.gsf.2011.06.004